Streptococcus agalactiae MprF synthesizes a novel cationic glycolipid and plays a role in brain entry and meningitis

Luke R. Joyce[1], Haider S. Manzer[2], Jéssica da C. Mendonça[2], Ricardo Villarreal[2], Kelly S. Doran[2*], Kelli L. Palmer[1*], and Ziqiang Guan[3*]

[1]Department of Biological Sciences, The University of Texas at Dallas, Richardson, TX, 75080

[2]Department of Immunology and Microbiology, University of Colorado School of Medicine, Aurora, CO, 80045

[3]Department of Biochemistry, Duke University Medical Center, Durham, NC, 27710

*Corresponding authors

Kelly S. Doran: Kelly.Doran@CUAnschutz.edu
12800 E. 19th Ave., Rm. P18-9105, Aurora, CO, 80045. (303-724-3539)

Kelli L. Palmer: Kelli.Palmer@UTDallas.edu
800 W Campbell Rd, BSB 12, Richardson, TX, 75080. (972-883-6014)

Ziqiang Guan: Ziqiang.Guan@Duke.edu
307 Research Drive, 240 Nanaline Duke, Durham, NC, 27710. (919-684-3005)

Keywords: Group B *Streptococcus*, Lipidomics, Glycolipid, Meningitis, MprF

Abstract

Multiple peptide resistance factor (MprF) is highly conserved in bacterial pathogens and is an attractive target for novel antimicrobials due to its important roles in bacterial virulence. We uncovered novel biochemical and pathophysiological functions of MprF in *Streptococcus agalactiae* (Group B *Streptococcus*; GBS), which is a common cause of meningitis and severe infection in newborns. Uniquely, GBS MprF catalyzes the synthesis of lysyl-glucosyl-diacylglyerol (Lys-Glc-DAG), a novel cationic glycolipid, and to a lesser extent, lysyl-phosphatidylglycerol (Lys-PG). We show that GBS MprF significantly lowers the GBS surface negative charge and increases GBS acid tolerance. Further, we demonstrate that GBS MprF promotes brain entry and meningeal inflammation, using a mouse model of GBS meningitis. These results expand our knowledge of MprF functions, and the pathogenesis of meningitis caused by GBS.

36

37 **Introduction**

38 *Streptococcus agalactiae* (Group B *Streptococcus*; GBS) is a Gram-positive, β-hemolytic
39 bacterium that colonizes the lower genital and gastrointestinal tracts of approximately
40 30% of healthy women (1, 2). GBS causes disease in healthy adults and pregnant woman
41 and opportunistically causes life-threatening neonatal infections such as meningitis,
42 sepsis, and pneumonia (3–7). GBS can be transmitted from colonized mothers to
43 newborns during natural childbirth, and due to the severity of the resulting diseases,
44 intrapartum antibiotic prophylaxis is prescribed for colonized pregnant women (8, 9). Even
45 with these measures, GBS is still a leading cause of neonatal meningitis that results in
46 long-lasting neurological effects in surviving infants (4–7).

47

48 Research on the pathogenesis of the GBS has mainly focused on cell wall-anchored or
49 secreted proteins and polysaccharides that aid in the attachment to and invasion of host
50 cells. The numerous attachment and virulence factors possessed by the GBS are
51 summarized in a recent review by Armistead *et al* 2019 (10). Comparatively little is known
52 about GBS cellular membrane lipids, even though the bacterial membrane is a critical site
53 for host-pathogen interactions. To our knowledge, the only characterization of GBS
54 phospholipids prior to our current study was the identification of the phospholipids
55 phosphatidylglycerol (PG), cardiolipin (CL), and lysyl-phosphatidylglycerol (Lys-PG) in
56 GBS (11, 12). Similarly, investigation into the glycolipids of the GBS membrane has
57 focused on di-glucosyl-diacylglycerol (Glc_2-DAG), which is the lipid anchor of the Type I
58 lipoteichoic acid, and its role in pathogenesis (13).

59

60 Previous genomic analyses of GBS have identified a homolog of MprF (multiple peptide
61 resistance factor) (14). MprF catalyzes the aminoacylation of the anionic phospholipid PG
62 in a range of Gram-positive and Gram-negative bacteria (15, 16). MprF is a membrane-
63 bound enzyme comprised of a N-terminal flippase domain (17) and a C-terminal catalytic
64 domain that catalyzes the aminoacylation of the glycerol group of PG by using aminoacyl-
65 tRNAs as amino acid donors (18–20). An important function of aminoacylation, and in
66 particular lysylation, of PG in bacterial membranes is to lower the net negative charge of
67 their cellular envelope. This protects them from cationic antimicrobial peptides (CAMPs)
68 produced by host immune systems and bacteriocins produced by competitor bacteria (15,
69 16).
70
71 In this study, we utilized normal phase liquid chromatography (NPLC) coupled with
72 electrospray ionization (ESI) high-resolution tandem mass spectrometry (HRMS/MS) to
73 characterize the GBS membrane lipid composition, and identified a novel cationic
74 glycolipid, lysyl-glucosyl-diacylglycerol (Lys-Glc-DAG), which comprises a major portion
75 of the GBS total lipid extract. While Lys-PG has been reported in a range of bacterial
76 species (21), Lys-Glc-DAG represents, to our knowledge, the first example of lysine
77 modification of a neutral glycolipid. By gene deletion and heterologous expression, we
78 demonstrate that the GBS MprF enzyme is responsible for the biosynthesis of both the
79 novel Lys-Glc-DAG and Lys-PG. Furthermore, we identify MprF as a contributing factor
80 to GBS pathogenesis, both *in vitro* and *in vivo*.
81

Results

Identification of Lys-Glc-DAG, a novel cationic glycolipid in GBS

To characterize the membrane lipids of GBS cultured in Todd-Hewitt Broth (THB), three clinical isolates of representative serotypes were used: COH1 (serotype III) (22) , A909 (serotype Ia) (23), and CNCTC 10/84 (serotype V) (24, 25). Lipid extraction was performed using an acidic Bligh-Dyer method (26–28), followed by lipidomic analysis by normal phase LC-ESI/MS performed in both positive and negative ion modes. Figure 1A shows the total ion chromatogram (TIC) of LC-ESI/MS of the lipid extract of COH1 in the negative mode. Common Gram-positive bacterial lipids were identified by negative ion ESI/MS/MS, including diacylglyercol (DAG), monohexosyldiacylglycerol (MHDAG), dihexosyldiacylglycerol (DHDAG), PG, lyso-phosphatidylglycerol (lyso-PG), CL, Lys-PG, phosphatidic acid (PA), and undecaprenyl phosphate (C_{55}-P) (Table 1).

Surprisingly, the positive TIC (Figure 1B) shows highly abundant peaks of unknown identity at the retention time ~25-29 min. These TIC peaks are derived from *m/z* 803.595, *m/z* 831.624, *m/z* 857.644, *m/z* 885.671 and *m/z* 913.703 ions (Figure 1C), which are indicative of a lipid with varying acyl chain lengths. These ions were interpreted as $[M+H]^+$, given their corresponding $[M-H]^-$ and $[M+Cl]^-$ ions were detected in the negative mode (not shown). The mass spectra and LC retention times of this unknown lipid do not match with any other bacterial lipids we have analyzed. Searching lipidomic databases by exact masses did not result in any matches. The unknown lipid was also observed in A909 and CNCTC 10/84 strains (Figure S1). To identify this unknown lipid, MS/MS was performed in both positive and negative ion modes.

105

106 Positive ion MS/MS spectrum of *m/z* 885.6 (the most abundant species with a molecular
107 mass of 884.6 Da) produced structurally informative fragments (Figure 1D). In particular,
108 the low-mass fragments *m/z* 84.045 and *m/z* 129.061 are indicators of the presence of
109 amino acids, with lysine being a strong possibility (29). The *m/z* 129 is proposed to be
110 formed from lysine by elimination of H_2O; it fragments further to produce *m/z* 84, a low
111 mass ion observed in the spectra of many lysine derivatives (29). The NH_3 loss peak
112 observed at *m/z* 868.6 resulted from the elimination of an amino group of the lysine side
113 chain. The accurate mass measurement of fragments indicates that lysine is linked to a
114 hexose moiety. Specifically, the exact mass difference between *m/z* 291.114 and *m/z*
115 129.056 is 162.053, which is in agreement with the elemental composition of a hexose
116 subunit ($C_6H_{10}O_5$, calculated mass 162.053). Negative ion MS/MS provided further
117 structural information. As shown in Figure 1E, MS/MS of the $[M-H]^-$ ion at *m/z* 883.6
118 produced a major fragment ion at *m/z* 145.08, which corresponds to a deprotonated
119 lysine. The *m/z* 255.2 and 281.2 ions are the carboxylic anions of palmitic (C16:0) and
120 oleic (C18:1) fatty acids, respectively, revealing the two acyl chains of the most abundant
121 molecular species (MW 884.6).

122

123 Based on the above MS/MS and exact mass measurement, we propose lysyl-glucosyl-
124 diacylglyerol (Lys-Glc-DAG) (Figure 1F) as the structure of this unknown lipid. The
125 assignment of glucose was based on the observation that glucosyl-diacylglycerol (Glc-
126 DAG), the precursor of Lys-Glc-DAG, is a major membrane component of GBS and other
127 streptococci (13, 30), as well as the results from an isotopic labeling experiment using a

128 ^{13}C-labeled glucose, described below. The chemical structure of Lys-Glc-DAG is
129 consistent with its chromatographic properties under normal phase LC conditions. Due to
130 the presence of both polar (glucose) and charged (lysine) groups which bind strongly with
131 the silica-based stationary phase, Lys-Glc-DAG has longer retention times than other
132 major lipids in GBS. Also, Lys-Glc-DAG consists of several molecular species with
133 different fatty acyl compositions. These different Lys-Glc-DAG molecular species have
134 slightly different retention times, giving rise to multiple, unresolved TIC peaks (~25-29
135 min). The observed and calculated exact masses of major Lys-Glc-DAG molecular ion
136 species are shown in Table S1.
137

138 **Isotopic incorporation of lysine and glucose into Lys-Glc-DAG**

139 To further confirm the lysine and glucose moieties of Lys-Glc-DAG, we carried out stable
140 isotope-labeling experiments by culturing COH1 in streptococcal defined medium (DM)
141 supplemented with either deuterated lysine or ^{13}C-labeled glucose. In the deuterated
142 lysine (lysine-*d4*), 4 hydrogen (1 Da) atoms across 2 of the carbon atoms are replaced
143 with deuterium (2 Da) atoms, thereby increasing the mass of lysine by 4 Da. Figure 2A
144 and 2B show the positive ion mass spectra of the $[M+H]^+$ ions of Lys-Glc-DAG species
145 extracted from cultures in DM and in DM supplemented with lysine-*d4*, respectively. The
146 incorporation of lysine-*d4* into Lys-Glc-DAG is reflected by a 4 Da mass shift between the
147 $[M+H]^+$ ions of the unlabeled Lys-Glc-DAG (blue dots) and the lysine-*d4*-labeled Lys-Glc-
148 DAG (red dots). The same 4 Da mass shift is observed in the negative ion mode: the $[M-$
149 $H]^-$ ion of unlabeled Lys-Glc-DAG (16:0/18:1) is observed at *m/z* 883.6, while the lysine-
150 *d4* containing Lys-Glc-DAG (16:0/18:1) is observed at *m/z* 887.6 (Figure S2A).

151 Furthermore, MS/MS of *m/z* 883.6 (Figure S2B) and *m/z* 887.6 (Figure S2C) produced
152 fragment ions at *m/z* 145 and *m/z* 149, corresponding to the deprotonated lysine and
153 lysine-*d4*, respectively. The molecular weight shift of lysine-*d4* incorporation is also
154 observed in Lys-PG (Figure S2D). The incorporation of lysine-*d4* is shown by a 4 Da mass
155 shift between the $[M+H]^+$ ions of *m/z* 887.6 unlabeled Lys-PG (blue dots) to the *m/z* 881.6
156 lysine-*d4*-labeled Lys-PG (red dots).
157
158 In D-Glucose (U-$^{13}C_6$), all six carbon (12 Da) atoms are replaced with carbon-13 atoms
159 (^{13}C), thereby increasing the mass of glucose by 6 Da. In contrast to lysine-*d4* labeling,
160 the molecular profile of Lys-Glc-DAG from ^{13}C-labeled glucose labeling is more complex.
161 This is because ^{13}C-labeled glucose is utilized by GBS not only to replace the glucose
162 moiety of Lys-Glc-DAG, but also to synthesize its fatty acyl chains via glycolysis. As
163 shown in Figure 2C, the *m/z* 885.6 $[M+H]^+$ ion of unlabeled Lys-Glc-DAG (16:0/18:1) is
164 shifted to a broader distribution of ion peaks ranging from *m/z* 894.7 to 910.7. The mass
165 shifts (numbers in red) indicate the numbers of total ^{13}C atoms being incorporated into
166 the Lys-Glc-DAG (16:0/18:1) molecule. To locate the incorporated ^{13}C atoms on Lys-Glc-
167 DAG, MS/MS was performed on one of the most abundant ion species. Figure S2E shows
168 the MS/MS spectrum of *m/z* 885.6 of Lys-Glc-DAG in THB and Figure S2F shows the
169 MS/MS spectrum of *m/z* 900.7 in DM supplemented with D-Glucose-$^{13}C_6$ (containing a
170 total of fifteen ^{13}C atoms). The replacement of glucose by D-Glucose (U-$^{13}C_6$) in Lys-Glc-
171 DAG is evidenced by a 6 Da mass shift of the lysyl-glucosyl moiety from *m/z* 291.1 (Figure
172 S2E) to *m/z* 297.1 (Figure S2F). The other nine ^{13}C atoms must be distributed in the
173 diacylglycerol portion of Lys-Glc-DAG. Furthermore, careful comparison of both MS/MS

174 spectra of labeled and unlabeled Lys-Glc-DAG indicates that the lysine residue is linked
175 to the 6-position of glucose; the fragmentation schemes for *m/z* 189.0 (no ^{13}C atoms)
176 (Figure S2E) and ^{13}C-labeled *m/z* 191.0 (two ^{13}C atoms) (Figure S2F) are indicated.
177

178 **Heterologous expression of GBS *mprF* in *S. mitis* results in the production of both**
179 **Lys-Glc-DAG and Lys-PG**

180 GBS encode an ortholog of MprF (14). MprF catalyzes the aminoacylation of PG to form
181 Lys-PG and other minor aminoacyl-PGs such as Ala-PG and Arg-PG in other bacterial
182 species (15, 16). Our identification of Lys-PG in the cellular membrane of the GBS
183 confirms that an active MprF is present in GBS.
184

185 To ascertain if the GBS MprF is responsible for the addition of lysine to Glc-DAG to form
186 Lys-Glc-DAG, a heterologous host expression system was designed in *Streptococcus*
187 *mitis* ATCC 49456, a *S. mitis* type strain. We selected *S. mitis* because it does not encode
188 *mprF* and it is naturally transformable. Moreover, our previous lipidomic analysis
189 confirmed that it does not synthesize Lys-PG, but does synthesize Glc-DAG, the
190 precursor of Lys-Glc-DAG, as a major membrane component (28, 31). The gene
191 encoding GBS COH1 *mprF*, GBSCOH1_1931, was cloned into pABG5Δ*phoZ* (32) for
192 expression (the empty vector is referred to as pABG5 hereafter). As controls, the two
193 *mprF* genes of *Enterococcus faecium* strain 1,231,410, EFTG_00601 (*mprF1*) and
194 EFTG_02430 (*mprF2*), were also cloned for expression in *S. mitis*. One *E. faecium mprF*
195 allele (*mprF1*) has been experimentally verified to direct synthesis of Lys-PG, while the
196 second one (*mprF2*) does not (18).

197

198 *S. mitis* strains were cultured overnight in THB before lipidomics was performed. Figure
199 3A-C shows the lipidomic profile of *S. mitis* (pABG5) (empty vector control), *S. mitis*
200 (pEfmMprF1), and *S. mitis* (pGBSMprF). In Figure 3, Panel 1 shows the TIC, Panel 2
201 shows the MS of the retention time 19.5 – 21.5 min expected for Lys-PG, and Panel 3
202 shows the MS of the retention time 26 – 30 min expected for Lys-Glc-DAG.
203 Phosphatidylcholine, a previously described membrane lipid in *S. mitis* (28), elutes off the
204 column at roughly the same time as Lys-PG. The empty vector control strain does not
205 synthesize Lys-PG (Figure 3A, Panel 2) or Lys-Glc-DAG (Figure 3A, Panel 3). In *S. mitis*
206 (pEfmMprF1), Lys-PG is observed in the membrane (Figure 3B, Panel 2) but no Lys-Glc-
207 DAG is present (Figure 3B, Panel 3), which is consistent with previous findings in *E.*
208 *faecium* (18). As expected, *S. mitis* (pEfmMprF2) does not produce Lys-PG (Figure S3).
209 Finally, *S. mitis* (pGBSMprF) synthesizes high levels of Lys-Glc-DAG, as shown by a
210 large TIC peak at 26 to 30 min (Figure 3C, Panel 1). MS spectra indicate Lys-PG is
211 present in the membrane (Figure 3C, Panel 2) and Lys-Glc-DAG is produced (Figure 3C,
212 Panel 3) with major molecular species at *m/z* 857 and *m/z* 885, which are also detected
213 in the GBS membrane. Taken together, these heterologous host expression results in *S.*
214 *mitis* reveal that GBS MprF not only synthesizes Lys-PG but also possesses the unique
215 and novel activity of modifying Glc-DAG to form Lys-Glc-DAG.

216

217 **Deletion of *mprF* in GBS results in the loss of synthesis of Lys-PG and Lys-Glc-**
218 **DAG**

219 To validate the function of MprF in the synthesis of Lys-Glc-DAG *in vivo* in GBS, we
220 deleted the *mprF* gene, GBSCOH1_1931, from the COH1 genome using the sucrose
221 sensitivity selection plasmid pMBSacB (33) and confirmed the deletion by whole genome
222 sequencing. Figure 4A Panel 1 shows COH1 wild-type (WT) TIC and the abundance of
223 Lys-PG (Figure 4A, Panel 2) and Lys-Glc-DAG (Figure 4A, Panel 3). The COH1Δ*mprF*
224 TIC shows a complete loss of Lys-PG and Lys-Glc-DAG (Figure 4B, Panel 1), supported
225 by the absence of ions of Lys-PG (Figure 4B, Panel 2) and Lys-Glc-DAG (Figure 4B,
226 Panel 3) in the corresponding ESI/MS spectra. The complemented strain, COH1Δ*mprF*
227 (pGBSmprF), has a TIC lipid profile similar to that of WT COH1 (Figure 4C, Panel 1) and
228 shows the restoration of both Lys-PG (Figure 4C, Panel 2) and Lys-Glc-DAG (Figure 4C,
229 Panel 3). Together, these data demonstrate that GBS MprF is responsible for
230 synthesizing both Lys-PG and Lys-Glc-DAG. While MprF is well-known to modify anionic
231 PG with lysine and other amino acids, to our knowledge, aminoacylation of a neutral lipid
232 has not been reported. Overall, these data conclusively demonstrate a novel function of
233 GBS MprF (Figure 5). These results also demonstrate that, even though Lys-Glc-DAG
234 makes up a relatively large proportion of the total lipid extract, it is non-essential for growth
235 under the laboratory conditions tested here.

236

237 **GBS synthesize lysine lipids in various physiological lysine concentrations.**

238 GBS are lysine auxotrophs (34). In the human host, L-lysine has been quantified in
239 varying concentrations throughout the body, from ~43 μM in cerebrospinal fluid to ~441

240 μM in blood (35). To confirm the production of Lys-PG and Lys-Glc-DAG under
241 physiologically relevant lysine concentrations, a lysine titration was performed in DM. At
242 50 μM lysine concentration, GBS growth was reduced and reached an overnight OD_{600nm}
243 of ~0.36 (compare to normal overnight growth of ~OD_{600nm} 1.75 with 600 μM lysine). Lys-
244 PG and Lys-Glc-DAG were always present in the GBS membrane, but their levels varied
245 in a lysine-dependent manner at concentrations ranging from 50 μM to 600 μM (Figure
246 6A and Figure S4A-D). These data demonstrate that considerable levels of Lys-PG and
247 Lys-Glc-DAG are present in the GBS membrane, even at the lower range of
248 physiologically relevant lysine concentrations.
249

250 **A GBS *mprF* mutant has altered cell surface charge, pH stress survival, and cellular**
251 **chain length**

252 Aminoacylated phospholipids synthesized by MprF, especially Lys-PG, reduce the
253 negative charges on the outer surface of the membrane and aid in survival under acidic
254 conditions in other bacteria (15, 16, 36, 37). To investigate the effects of MprF activity on
255 the GBS membrane surface charge, Cytochrome C binding assays were performed.
256 Cytochrome C is positively charged, and more Cytochrome C bound to bacterial cells
257 indicates a greater net negative outer surface charge. The Δ*mprF* mutant bound
258 significantly more Cytochrome C compared to WT COH1 and complement strains (Figure
259 6B). The difference between the GBS WT and Δ*mprF* mutant is ~25%, which is less than
260 what is observed for *S. aureus* WT/Δ*mprF* mutant comparisons (~70%) under different
261 growth and assay conditions (38, 39). To assess the ability of the Δ*mprF* mutant to survive
262 in acidic conditions, a growth assay in pH-adjusted media was performed. The growth of

263 the Δ*mprF* mutant was reduced at a pH of 5.5, and the mutant failed to grow at pH 5,
264 compared to WT COH1 and complement strains (Figure 6C). Finally, given the substantial
265 membrane charge alteration in the Δ*mprF* mutant (Figure 6B), we assessed whether
266 *mprF* deletion altered the cell morphology and/or division phenotype. Confocal
267 microscopy with a membrane dye was performed on overnight cultures. It was observed
268 that the Δ*mprF* mutant grew in significantly longer chains compared to WT COH1 (Figure
269 6D). Finally, *mprF* deletion did not impact GBS hemolytic activity (Figure S4E), and there
270 was no difference in growth observed between COH1(pABG5), COH1Δ*mprF*(pABG5),
271 and COH1Δ*mprF*(pGBSMprF) strains in THB medium *in vitro* (Figure S4F). Taken
272 together, these results indicate important physiological roles for MprF in GBS.
273

274 **MprF contributes to GBS interactions with human cells *in vitro***

275 Next, we determined whether loss of MprF altered host cell interaction. To mimic the
276 human blood-brain barrier (BBB), the human cerebral microvascular endothelial cell line
277 hCMEC/D3 was utilized. The *in vitro* assays for adhesion and invasion were performed
278 using pre-established protocols (40, 41). To control for the presence of the plasmid
279 backbone in the complement strain, COH1(pABG5), COH1Δ*mprF*(pABG5), and
280 COH1Δ*mprF*(pGBSMprF) strains were used. There was no significant difference in the
281 number of Δ*mprF* mutant compared to WT and complement cells attached to hCMEC/D3
282 cells (Figure S5A). However, Figure 7A shows a significant decrease in the number of
283 Δ*mprF* mutant cells able to invade the hCMEC/D3 cells. Interestingly, the Δ*mprF* mutant
284 had a significant decrease in the ability to both adhere and invade the human vaginal
285 epithelial cell line VK2/E6E7 (Figure S5B and S5C). When calculating the percentage of

286 VK2/E6E7-associated GBS that had invaded the cell, the differences in recovered
287 intracellular bacteria were not significant (Figure S5D), suggesting that in this cell type
288 MprF contributes more to bacterial attachment. Taken together, these data indicate that
289 MprF promotes the ability of GBS to invade host cells and attach to certain cell types.
290

291 **The GBS MprF is important for the development of meningitis *in vivo***

292 Our results suggest that MprF contributes to GBS invasion into brain endothelial cells.
293 We hypothesized that this *in vitro* phenotype would translate into a diminished ability to
294 penetrate the BBB and produce meningitis *in vivo*. Using our standard model of GBS
295 hematogenous meningitis, mice were challenged with either WT GBS or the Δ*mprF*
296 mutant as described in the Methods (13, 40–43). Mice were sacrificed at a defined
297 endpoint (72 h) to determine bacterial loads in blood and brain tissue. We recovered
298 significantly less CFU in the brains of COH1Δ*mprF*-infected mice compared to the COH1-
299 infected mice (Figure 7B). However, there was no significant difference in CFU recovered
300 from the bloodstream between WT and mutant infected mice, which demonstrates that
301 the Δ*mprF* mutant does not have generally diminished survival *in vivo* when in contact
302 with the mouse immune system (Figure 7C). To assess the level of inflammation, we
303 performed histological analysis of brains from infected animals. In WT-infected mice, we
304 observed leukocyte infiltration and meningeal thickening characteristic of meningitis,
305 which was less pronounced in the mice infected with the Δ*mprF* mutant strain (Figure
306 7D). Meningeal thickening was quantified as described in the Methods (Figure 7E).
307 Furthermore, consistent with these results, we observed that mice challenged with WT
308 GBS had significantly more neutrophil chemokine, KC, in brain homogenates compared

309 to Δ*mprF* mutant-infected animals (Figure 7F). Taken together, these data indicate that
310 *mprF* contributes to GBS penetration into the brain and to the pathogenesis of meningitis
311 *in vivo*.
312

313 **Discussion**

314 The cellular membrane is a critical site of interaction between Gram-positive pathogens
315 and their hosts. In this study, we used LC-ESI/MS to characterize the lipid membranes of
316 multiple serotypes of GBS. We identified Lys-Glc-DAG, a novel lysine modification on the
317 glycolipid Glc-DAG, which comprises a relatively large proportion of the cellular lipid
318 extract of these strains. To our knowledge, this is the first description of the lysynylated
319 glycolipid, Lys-Glc-DAG. We found that MprF is responsible for the addition of lysine to
320 both Glc-DAG and PG, thus establishing a novel glycolipid (glucosyl-DAG) substrate for
321 MprF. We identified that MprF activity contributes to important physiological features of
322 the GBS cellular membrane, including pH stress survival and the modulation of cell
323 surface charge and cellular chain length. We further demonstrate that GBS MprF
324 promotes invasion into brain endothelium and contributes to the development of CNS
325 disease in a mouse model of experimental meningitis.
326

327 We found that both Lys-Glc-DAG and Lys-PG are synthesized by the GBS MprF.
328 Decoupling the synthesis of Lys-PG and Lys-Glc-DAG will allow for identification of the
329 specific roles each lipid plays in GBS physiology and pathogenesis. We previously
330 analyzed *E. faecium* lipids with the same methods used here and confirmed that *E.*
331 *faecium* synthesizes Lys-PG but not Lys-Glc-DAG (44). We attempted to decouple the

332 synthesis of Lys-Glc-DAG and Lys-PG in GBS by expressing *E. faecium mprF1* (from
333 pEFMprF1 used in *S. mitis* expression studies in Figure 3) in the GBS Δ*mprF* mutant but
334 were unable to obtain transformants. An alternative strategy will be to use previously
335 reported MprF C-terminal domain crystal structures from *Bacillus* and *Pseudomonas* (19)
336 to identify residues likely to be important for GBS lipid substrate flexibility, or, in a less
337 targeted approach, alanine scanning mutagenesis. However, our difficulty in obtaining
338 transformants for pEFMprF1, which was readily transformable into *S. mitis*, in the GBS
339 Δ*mprF* mutant, which was readily transformable by other plasmids with the same
340 backbone, suggests that a delicate balance between Lys-PG and Lys-Glc-DAG is
341 required for GBS. It is interesting to note that, depending on lysine availability, GBS
342 produce far more Lys-Glc-DAG than Lys-PG, as judged by LC/MS analysis. It is possible
343 that that Lys-Glc-DAG can be more effectively used to modulate the charge-related
344 biophysical and physiological properties of GBS membrane than Lys-PG.
345
346 Synthesis of Lys-PG and Lys-Glc-DAG by MprF requires amino acid, glycolipid, and
347 phospholipid substrates. Lys-tRNAs are required by translational machinery for protein
348 synthesis and are essential for survival. Unlike *S. aureus*, a canonical organism for
349 studying MprF function, GBS are lysine auxotrophs (34). Therefore, in GBS, MprF and
350 the ribosome compete for lysine scavenged from the environment. Moreover, the
351 glycolipid Glc-DAG is a substrate for both MprF and Type I lipoteichoic acid (LTA)
352 biosynthesis. LTA is a critical polymer for binding host cells, repulsion of CAMPs, and is
353 required for invasion of the BBB (2, 13, 45). Whether MprF and LTA biosynthesis compete
354 for Glc-DAG, and by extension whether *mprF* deletion leads to increased LTA production,

355 remain to be determined. Finally, GBS MprF uses two lipid substrates, PG and Glc-DAG,
356 to synthesize two distinct lysine-modified lipids, the levels of all of which must be balanced
357 to maintain appropriate membrane charge. In *E. faecium*, the hydrolase encoded
358 immediately upstream of *mprF* is responsible for Lys-PG turnover in the membrane, thus
359 balancing the ratio of PG to Lys-PG present (36). A similar mechanism is likely present in
360 GBS. Indeed, GBSCOH1_1932, immediately upstream of the GBS *mprF*, encodes the
361 hydrolase domain MhpC (COG0596). This enzyme may regulate Lys-PG and/or Lys-Glc-
362 DAG levels in the membrane.
363
364 Why did GBS evolve to use MprF to lysinylate Glc-DAG? The use of such an important
365 substrate, required by GBS for protein synthesis, to decorate the extracellular cell surface
366 is intriguing, especially under low lysine conditions *in vivo*. One possible explanation is to
367 mask the recognition of Glc-DAG, an experimentally verified microbial antigen, from
368 natural killer T cells (46, 47). A second possible explanation is to increase resistance to
369 neutrophil killing, as Lys-PG confers resistance to CAMPs in *S. aureus* (15). However, a
370 role for GBS MprF in CAMP resistance was not observed in a previous study *in vitro* (14),
371 and in this study the GBS Δ*mprF* mutant survived as well as the WT *in vivo* in the murine
372 bloodstream, suggesting that GBS *mprF* does not contribute generally to immune system
373 evasion. Acid stress response that is potentially greater with both lipids versus Lys-PG
374 alone, may increase the survival time in phagosomes where acidification is critical for
375 bacterial killing (48). In addition, human vaginal tract colonization requires survival in low
376 pH, as healthy adults have a pH range of 4.2 – 5, and the protective commensal
377 *Lactobacillus* is known to acidify the surrounding environment (49, 50). We show *in vitro*

378 that GBS MprF plays a critical role in survival at pH 5 and is important for interactions with
379 human vaginal epithelial cells. These data suggest that MprF is especially important in
380 the niches GBS colonizes. The decreased *in vivo* pathogenicity of the Δ*mprF* mutant
381 presented in this work, identifies the GBS MprF as a strong candidate for targeting by
382 antimicrobial strategies recently described in *S. aureus* (17, 51). The fact that Lys-Glc-
383 DAG is a unique and major membrane component of GBS holds promise that Lys-Glc-
384 DAG could be utilized as a specific and efficient molecular biomarker for a rapid GBS
385 diagnostic test that would not rely on culturing procedures or nucleic acid amplification.
386
387 Overall, our work underscores the important roles of membrane lipids in pathogen-host
388 interactions. Our identification of the novel Lys-Glc-DAG glycolipid and the role MprF
389 plays in GBS disease pathogenesis rationalizes further study of the lipidomes of human
390 pathogens.
391

392 **Materials and methods**

393 **Bacterial strains, media, and growth conditions**

394 Strains and plasmids used in this study are shown in Table S2. GBS strains were grown
395 statically at 37°C in Todd-Hewitt Broth (THB) and *S. mitis* strains were grown statically at
396 37°C and 5% CO_2, unless otherwise stated. Streptococcal chemically defined medium
397 (52) was diluted from stock as described (53) with 1% w/v glucose (referred to as DM),
398 slightly modified from (54), unless otherwise stated. *Escherichia coli* strains were grown
399 in Lysogeny Broth (LB) at 37°C with rotation at 225 rpm. Kanamycin and erythromycin

400 (Sigma-Aldrich) were supplemented to media at 50 µg/mL and 300 µg/mL for *E. coli,*
401 respectively, or 300 µg/mL and 5 µg/mL, respectively, for streptococcal strains.
402
403 **Routine molecular biology techniques**
404 All PCR reactions utilized Phusion polymerase (Thermo Fisher) and all primers are shown
405 in Table S3. PCR products and restriction digest products were purified using GeneJET
406 PCR purification kit (Thermo Fisher) per manufacturer protocols. Plasmids were extracted
407 using GeneJET plasmid miniprep kit (Thermo Fisher) per manufacturer protocols.
408 Restriction enzyme digests utilized XbaI, XhoI, and PstI (New England Biolabs) for 3 h at
409 37°C in a water bath. Ligations utilized T4 DNA ligase (New England Biolabs) at 16°C
410 overnight or Gibson Assembly Master Mix (New England Biolabs) per manufacturer
411 protocols where stated. All plasmid constructs were sequence confirmed by Sanger
412 sequencing (Massachusetts General Hospital DNA Core).
413
414 **Deuterated lysine and $^{13}C_6$-D-glucose isotope tracking**
415 A GBS COH1 colony was inoculated into 15 mL of DM containing 450 µM lysine-*d4*
416 (Cambridge Isotopes Laboratories) or a single COH1 colony was inoculated into 10 mL
417 DM supplemented with 0.5% w/v $^{13}C_6$D-glucose (U-13C6, Cambridge Isotopes
418 Laboratories) for overnight growth for lipidomic analysis described below.
419
420 **Construction of MprF expression and *mprF* deletion plasmids**
421 For expression plasmids, the *mprF* genes from GBS COH1, (GBSCOH1_1931), and *E.*
422 *faecium* 1,231,410 (EFTG_00601 and EFTG_02430) were amplified and Gibson ligated

423 into pABG5Δ*phoZ* (32) transformed and maintained in *E. coli* DH5α cells with 50 µg/mL
424 kanamycin. The gene deletion plasmid was constructed by amplifying regions ~ 2 kb
425 upstream and downstream of the GBS COH1 *mprF* (GBSCOH1_1931), digested with
426 appropriate restrictions enzymes indicated on the primers (Table S3), and ligated
427 overnight into the similarly digested plasmid, pMBSacB (33). The knockout plasmid was
428 transformed and maintained in *E. coli* DH5α at 28°C with 300 µg/mL erythromycin.
429 Plasmids were extracted and sequence-verified as described above. For more
430 information see Supplementary Text S1.
431

432 **Expression of *mprF* in *S. mitis***

433 Natural transformation was performed as previously described (28). Briefly, precultures
434 were thawed at room temperature, diluted in 900 µL of THB, further diluted 1:50 in
435 prewarmed 5 mL THB, and incubated for 45 min at 37°C. 500 µL of culture was then
436 aliquoted with 1 µL of 1 mg/ml competence-stimulating peptide (EIRQTHNIFFNFFKRR)
437 and 1 µg/mL plasmid. Transformation reaction mixtures were cultured for 2 h at 37°C in
438 microcentrifuge tubes before being plated on THB agar supplemented with 300 µg/mL
439 kanamycin. Single transformant colonies were cultured in 15 mL THB overnight. PCR
440 was used to confirm the presence of the *mprF* insert on the plasmid. Plasmids were
441 extracted and sequence confirmed as described above. Lipidomics was performed as
442 described below in biological triplicate.
443

444 **Deletion of GBS COH1 *mprF***

445 Electrocompetent cells were generated as described (33) with minor modifications, see
446 Supplemental Text S1 for more detail. The double crossover homologous recombination
447 knockout strategy was performed as described previously (33, 40, 55) with minor
448 modifications. 1 µg of plasmid was added to electrocompetent COH1 cells and transferred
449 to a cold 1 mm cuvette (Fisher). Electroporation was carried out at 2.5 kV on an Eppendorf
450 eporator. 1 mL of THB containing 12.5% PEG 8000, 20 mM $MgCl_2$, and 2 mM $CaCl_2$ was
451 immediately added and then the entire reaction was transferred to a glass culture tube.
452 Outgrowth was at 28°C for 2 h followed by plating on THB agar supplemented with 5
453 µg/mL erythromycin. Plates were incubated for 48 h at 28°C. A single colony was cultured
454 overnight in 5 mL THB with 5 µg/mL erythromycin at 28°C. The culture was screened via
455 PCR for the plasmid insert with the initial denaturing step extended to 10 min. The
456 overnight culture was diluted 1:1000 THB containing 5 µg/mL erythromycin and incubated
457 overnight at 37°C to promote single cross over events. The culture was then serial diluted
458 and plated on THB agar plates with antibiotic and incubated at 37°C overnight. Colonies
459 were screened for single crossover events by PCR (Table S3). Single crossover colonies
460 were inoculated in 5 mL THB at 28°C to promote double crossover events. Overnight
461 cultures were diluted 1:1000 into 5 mL THB containing sterile 0.75 M sucrose and
462 incubated at 37°C. Overnight cultures were serial diluted and plated on THB agar and
463 incubated at 37°C overnight. Colonies were patched onto THB agar with and without 5
464 µg/mL erythromycin to confirm loss of plasmid. Colonies were also screened by PCR for
465 the loss of *mprF*. Colonies positive for the loss of *mprF* were inoculated into 5 mL THB at
466 37°C. Cultures were stocked and gDNA extracted as described above, with minor

467 modifications. Sequence confirmation of the *mprF* knockout was done via Sanger
468 sequencing (Massachusetts General Hospital DNA Core) using primers in Table S2. The
469 mutant was grown overnight in 15 mL THB at 37°C and pelleted at 6,150 x *g* for 5 min in
470 a Sorvall RC6+ centrifuge at room temperature for lipid extraction as described. Genomic
471 DNA of COH1Δ*mprF* was isolated as described above and whole genome sequencing
472 was performed in paired-end reads (2 by 150 bp) on the Illumina NextSeq 550 platform
473 at the Microbial Genome Sequencing Center (Pittsburgh, PA).
474
475 **Complementation of *mprF* in COH1Δ*mprF***
476 Electrocompetent COH1Δ*mprF* were generated as previously described (56).
477 Electroporation was performed as described above, with recovery in THB supplemented
478 with 0.25 M sucrose, and plated on THB agar with kanamycin at 300 µg/mL. Biological
479 triplicate complementation strains were grown overnight in THB with kanamycin before
480 lipidomics was performed as described. See Text S1 for more detail.
481
482 **Acidic Bligh-Dyer extractions**
483 Centrifugation was performed using a Sorvall RC6+ centrifuge. Cultures were pelleted at
484 4,280 x *g* for 5 min at room temperature unless otherwise stated. The supernatants were
485 removed, and cell pellets were stored at -80°C until acidic Bligh-Dyer lipid extractions
486 were performed as described (28). See Text S1 for more information.
487

488 **Liquid Chromatography/Electrospray Ionization Mass Spectrometry**

489 Normal phase LC was performed on an Agilent 1200 quaternary LC system equipped
490 with an Ascentis silica HPLC column (5 µm; 25 cm by 2.1 mm; Sigma-Aldrich) as
491 described previously (27, 57). See Text S1 for more information.

492

493 **Cytochrome C assay**

494 Cytochrome C assay was performed as described previously (58, 59) with minor
495 modifications. Briefly, overnight cultures of strains were diluted to an OD_{600nm} of 0.05 in
496 20 mL prewarmed THB, with no antibiotic, and grown to mid exponential phase (OD_{600nm}
497 between 0.48 – 0.6) before cells were pelleted to an OD_{600nm} of 7 in 1 mL and washed
498 twice with morpholinepropanesulfonic acid (MOPS) at pH 7. Cells were resuspended in
499 1 mg/mL Cytochrome C (Sigma) in MOPS buffer and incubated for 10 min at room
500 temperature. Cells were pelleted at 16,000 x *g* for 3 min in a tabletop centrifuge,
501 supernatant transferred to disposable spectrophotometer cuvette (Fisher), and
502 absorbance read at 535nm (A_{535}) using a Thermo Scientific Genesys 30
503 spectrophotometer. The control A_{535} was 1 mg/mL Cytochrome C in MOPS buffer with no
504 cells present, which was also incubated and centrifuged. % unbound was calculated using
505 the following formula: ((A_{535}/Control A_{535}) * 100) and WT was set to 100%. Biological
506 triplicate was used for each strain.

507

508 **pH-adjusted THB growth**

509 Approximately 30 mL of fresh THB were adjusted to different pH values, measured using
510 a Mettler Toledo FiveEasy pH/MV meter, and sterile-filtered using 0.22 µM syringe filters.

511 A final volume of 200 µL culture medium was aliquoted per well in a flat-bottom 96 well
512 plate (Falcon); culture media were not supplemented with antibiotics. Overnight cultures
513 of GBS strains were used to inoculate the wells to a starting OD_{600nm} 0.02 per well. Plates
514 were incubated for 24 h at 37°C before OD_{600nm} was read using a BioTek MX Synergy 2
515 plate reader. This experiment was performed in biological triplicate.
516

517 **Membrane dye and imaging of GBS**

518 Overnight cultures were gently resuspended 5 times by pipette. 19 µL culture was
519 removed into sterile Eppendorf tubes. 1 µL of 1 µg/mL FM4-64 (N-(3-
520 Triethylammoniumpropyl)-4-(6-(4-(Diethylamino) Phenyl) Hexatrienyl) Pyridinium
521 Dibromide) membrane dye (Invitrogen) was added to each tube. The culture and dye
522 were dropped onto a 0.75 mm 0.75% agarose pad and allowed to stand for 5 min. Cover
523 slips were placed and sealed. A Zeiss LSM 880 confocal microscope was used for
524 imaging with 100X objective, oil immersion, and laser excitation at 561 nm. Settings of
525 laser power 1%, gain 750, digital offset 0 and digital gain 1 were used for each image.
526 Five representative images were taken from each slide and the number of diplococci
527 occurring in each chain was manually counted.
528

529 **hCMEC and VK2 cell adherence and invasion assays**

530 Human Cerebral Microvascular Endothelial cells hCMEC/D3 (obtained from Millipore)
531 were grown in EndoGRO-MV complete media (Millipore, SCME004) supplemented with
532 5% fetal bovine serum (FBS) and 1 ng/ml fibroblast growth factor-2 (FGF-2; Millipore).
533 Human vaginal epithelial VK2/E6E7 (obtained from American Type Culture Collection

534 (ATCC) (CRL-2616)) cells were grown in keratinocyte serum-free medium (KSFM)
535 (Gibco) supplemented with 0.5 ng/mL human recombinant epidermal growth factor and
536 0.05 mg/mL bovine pituitary extract. Cells were grown in tissue culture treated 24 well
537 plates and 5% CO_2 at 37°C.
538
539 Assays to determine the total number of bacteria adhered to host cells or intracellular
540 bacteria were performed as described previously (40, 41). Briefly, bacteria were grown to
541 mid log phase (OD_{600nm} 0.4-0.5) and normalized to 1 x 10^8 to infect cell monolayers at a
542 multiplicity of infection (MOI) of 1 (1 x 10^5 CFU per well). The total cell-associated GBS
543 were recovered after 30 min incubation. Cells were washed slowly five times with 500 µL
544 1X PBS (Sigma) and detached by addition of 100 µL of 0.25% trypsin-EDTA solution
545 (Gibco) and incubation for 5 min before lysing the eukaryotic cells with the addition of 400
546 µL of 0.025% Triton X-100 (Sigma) and vigorous pipetting. The lysates were then serially
547 diluted and plated on THB agar and incubated overnight to determine CFU. Bacterial
548 invasion assays were performed as described above except infection plates were
549 incubated for 2 h before incubation with 100 µg gentamicin (Sigma) and 5 µg penicillin
550 (Sigma) supplemented media for an additional 2 h to kill all extracellular bacteria, prior to
551 being trypsinized, lysed, and plated as described. Experiments were performed in
552 biological triplicate with four technical replicates per experiment.
553
554 **Murine model of GBS hematogenous meningitis**
555 All animal experiments were conducted under the approval of the Institutional Animal
556 Care and Use Committee (#00316) at the University of Colorado Anschutz Medical

557 Campus and performed using accepted veterinary standards. The murine meningitis
558 model was performed as previously described (40, 42, 43). Briefly, 7-week-old male
559 CD1 (Charles River) mice were challenged intravenously with 1×10^9 CFU of WT COH1
560 or the isogenic Δ*mprF* mutant. At 72 h post-infection, mice were euthanized and blood
561 and brain tissue were harvested, homogenized, and serially diluted on THB agar plates
562 to determine bacterial CFU.
563

564 **Histology and ELISA**

565 Mouse brain tissue was frozen in OCT compound (Sakura) and sectioned using a
566 CM1950 cryostat (Leica). Sections were stained using hematoxylin and eosin (Sigma)
567 and images were taken using a BZ-X710 microscope (Keyence). Images were analyzed
568 using ImageJ software. Meningeal thickening was quantified from sections taken from
569 three different mice per group, and six images per slide. Meningeal thickening was
570 quantified across two points per image. KC protein from mouse brain homogenates was
571 detected by enzyme-linked immunosorbent assay according to the manufacturer's
572 instructions (R&D systems).
573

574 **Statistical analyses**

575 All statistical analyses were performed using GraphPad Prism version 8 for Windows,
576 GraphPad Software, La Jolla California USA, www.graphpad.com.
577

578 **Accession numbers**

579 Illumina sequence reads generated in this study have been deposited in the Sequence
580 Read Archive under accession PRJNA675025.

581

582 **Conflict of interest**

583 The authors have declared that no conflict of interest exists.

584

585 **Acknowledgements**

586 We gratefully acknowledge Kathryn Patras at the University of California San Diego for
587 the CNCTC 10/84 strain and Moutusee Islam in Kelli Palmer's lab at The University of
588 Texas at Dallas for the *E. faecium* 1,231,410 genomic DNA used for PCR amplification.

589

590 The work was supported in part by T32 5T32AI052066-18 for H.S.M, the Coordenação
591 de Aperfeiçoamento de Pessoal de Nível Superior, Brazil (CAPES; finance code 001 to
592 J.D.C.M), by grant R01NS116716 from the National Institutes of Health to K.S.D and
593 associated supplement from NINDS to R.V., by grant R21AI130666 from the National
594 Institutes of Health and the Cecil H. and Ida Green Chair in Systems Biology Science to
595 K.P, grant R56AI139105 from the National Institutes of Health to K.P and Z.G, and grant
596 U54GM069338 from the National Institutes of Health to Z.G.

597

598 **References**

599 1. Wilkinson HW. 1978. Group B Streptococcal Infection in Humans. Annu Rev
600 Microbiol 32:41–57.

601 2. Doran KS, Nizet V. 2004. Molecular pathogenesis of neonatal Group B

602 Streptococcal infection: No longer in its infancy. Mol Microbiol 54:23–31.
603 3. Hall J, Adams NH, Bartlett L, Seale AC, Lamagni T, Bianchi-Jassir F, Lawn JE,
604 Baker CJ, Cutland C, Heath PT, Ip M, Le Doare K, Madhi SA, Rubens CE, Saha
605 SK, Schrag S, Sobanjo-Ter Meulen A, Vekemans J, Gravett MG. 2017. Maternal
606 Disease With Group B *Streptococcus* and Serotype Distribution Worldwide:
607 Systematic Review and Meta-analyses. Clin Infect Dis 65:S112–S124.
608 4. Schuchat A. 1999. Group B *Streptococcus*. Lancet 353:51–56.
609 5. Campbell JR, Hillier SL, Krohn MA, Ferrieri P, Zaleznik DF, Baker CJ. 2000.
610 Group B Streptococcal colonization and serotype-specific immunity in pregnant
611 women at delivery. Obstet Gynecol 96:498–503.
612 6. Nandyal RR. 2008. Update on Group B Streptococcal infections: perinatal and
613 neonatal periods. J Perinat Neonatal Nurs 22:230–7.
614 7. Edwards MS, Rench MA, Haffar AA, Murphy MA, Desmond MM, Baker CJ. 1985.
615 Long-term sequelae of Group B Streptococcal meningitis in infants. J Pediatr
616 106:717–22.
617 8. Schuchat A. 1998. Epidemiology of Group B Streptococcal disease in the United
618 States: shifting paradigms. Clin Microbiol Rev 11:497–513.
619 9. Ohlsson A, Shah VS. 2014. Intrapartum antibiotics for known maternal Group B
620 Streptococcal colonization. Cochrane database Syst Rev CD007467.
621 10. Armistead B, Oler E, Adams Waldorf K, Rajagopal L. 2019. The Double Life of
622 Group B *Streptococcus*: Asymptomatic Colonizer and Potent Pathogen. J Mol Biol
623 431:2914–2931.
624 11. Curtis J, Kim G, Wehr NB, Levine RL. 2003. Group B Streptococcal phospholipid

625 causes pulmonary hypertension. Proc Natl Acad Sci U S A 100:5087–90.
626 12. Fischer W. 1977. The polar lipids of Group B Streptococci. II. Composition and
627 positional distribution of fatty acids. Biochim Biophys Acta 487:89–104.
628 13. Doran KS, Engelson EJ, Khosravi A, Maisey HC, Fedtke I, Equils O, Michelsen
629 KS, Arditi M, Peschel A, Nizet V. 2005. Blood-brain barrier invasion by group B
630 *Streptococcus* depends upon proper cell-surface anchoring of lipoteichoic acid. J
631 Clin Invest 115:2499–507.
632 14. Saar-Dover R, Bitler A, Nezer R, Shmuel-Galia L, Firon A, Shimoni E, Trieu-Cuot
633 P, Shai Y. 2012. D-alanylation of lipoteichoic acids confers resistance to cationic
634 peptides in Group B *Streptococcus* by increasing the cell wall density. PLoS
635 Pathog 8:e1002891.
636 15. Peschel A, Jack RW, Otto M, Collins LV, Staubitz P, Nicholson G, Kalbacher H,
637 Nieuwenhuizen WF, Jung G, Tarkowski A, Van Kessel KPM, Van Strijp JAG.
638 2001. *Staphylococcus aureus* resistance to human defensins and evasion of
639 neutrophil killing via the novel virulence factor MprF is based on modification of
640 membrane lipids with L-lysine. J Exp Med 193:1067–1076.
641 16. Roy H, Ibba M. 2008. RNA-dependent lipid remodeling by bacterial multiple
642 peptide resistance factors. Proc Natl Acad Sci U S A 105:4667–4672.
643 17. Ernst CM, Kuhn S, Slavetinsky CJ, Krismer BB, Heilbronner S, Gekeler C, Kraus
644 D, Wagner S, Peschel A. 2015. The Lipid-Modifying Multiple Peptide Resistance
645 Factor Is an Oligomer Consisting of Distinct Interacting Synthase and Flippase
646 subunits. MBio 6:1–9.
647 18. Roy H, Ibba M. 2009. Broad range amino acid specificity of RNA-dependent lipid

648 remodeling by multiple peptide resistance factors. J Biol Chem 284:29677–29683.
649 19. Hebecker S, Krausze J, Hasenkampf T, Schneider J, Groenewold M, Reichelt J,
650 Jahn D, Heinz DW, Moser J. 2015. Structures of two bacterial resistance factors
651 mediating tRNA-dependent aminoacylation of phosphatidylglycerol with lysine or
652 alanine. Proc Natl Acad Sci U S A 112:10691–10696.
653 20. Lennarz WJ, Nesbitt JA, Reiss J. 1966. The participation of sRNA in the
654 enzymatic synthesis of O-L-lysyl phosphatidylgylcerol in *Staphylococcus aureus*.
655 Proc Natl Acad Sci U S A 55:934–941.
656 21. Slavetinsky C, Kuhn S, Peschel A. 2017. Bacterial aminoacyl phospholipids -
657 Biosynthesis and role in basic cellular processes and pathogenicity. Biochim
658 Biophys acta Mol cell Biol lipids 1862:1310–1318.
659 22. Kuypers JM, Heggen LM, Rubens CE. 1989. Molecular analysis of a region of the
660 Group B *Streptococcus* chromosome involved in type III capsule expression.
661 Infect Immun 57:3058–65.
662 23. Lancefield RC, McCarty M, Everly WN. 1975. Multiple mouse-protective
663 antibodies directed against Group B Streptococci. Special reference to antibodies
664 effective against protein antigens. J Exp Med 142:165–79.
665 24. Wilkinson HW. 1977. Nontypable Group B Streptococci isolated from human
666 sources. J Clin Microbiol 6:183–4.
667 25. Hooven TA, Randis TM, Daugherty SC, Narechania A, Planet PJ, Tettelin H,
668 Ratner AJ. 2014. Complete Genome Sequence of *Streptococcus agalactiae*
669 CNCTC 10/84, a Hypervirulent Sequence Type 26 Strain. Genome Announc 2.
670 26. Bligh EG, Dyer WJ. 1959. A Rapid Method of Total Lipid Extraction and

671 Purification. Can J Biochem Physiol 37:911–917.
672 27. Tan BK, Bogdanov M, Zhao J, Dowhan W, Raetz CRH, Guan Z. 2012. Discovery
673 of a cardiolipin synthase utilizing phosphatidylethanolamine and
674 phosphatidylglycerol as substrates. Proc Natl Acad Sci 109:16504–16509.
675 28. Joyce LR, Guan Z, Palmer KL. 2019. Phosphatidylcholine Biosynthesis in Mitis
676 Group Streptococci via Host Metabolite Scavenging. J Bacteriol 201:e00495-19.
677 29. Yalcin T, Harrison AG. 1996. Ion chemistry of protonated lysine derivatives. J
678 Mass Spectrom 31:1237–43.
679 30. Meiers M, Volz C, Eisel J, Maurer P, Henrich B, Hakenbeck R. 2014. Altered lipid
680 composition in *Streptococcus pneumoniae* cpoA mutants. BMC Microbiol 14:1–
681 12.
682 31. Adams HM, Joyce LR, Guan Z, Akins RL, Palmer KL. 2017. *Streptococcus mitis*
683 and *S. oralis* Lack a Requirement for CdsA, the Enzyme Required for Synthesis of
684 Major Membrane Phospholipids in Bacteria. Antimicrob Agents Chemother
685 61:e02552-16.
686 32. Granok AB, Parsonage D, Ross RP, Caparon MG. 2000. The RofA binding site in
687 *Streptococcus pyogenes* is utilized in multiple transcriptional pathways. J
688 Bacteriol 182:1529–40.
689 33. Hooven TA, Bonakdar M, Chamby AB, Ratner AJ. 2019. A Counterselectable
690 Sucrose Sensitivity Marker Permits Efficient and Flexible Mutagenesis in
691 *Streptococcus agalactiae*. Appl Environ Microbiol 85:1–13.
692 34. Milligan TW, Doran TI, Straus DC, Mattingly SJ. 1978. Growth and amino acid
693 requirements of various strains of Group B Streptococci. J Clin Microbiol 7:28–33.

694 35. Wishart DS, Feunang YD, Marcu A, Guo AC, Liang K, Vázquez-Fresno R, Sajed
695 T, Johnson D, Li C, Karu N, Sayeeda Z, Lo E, Assempour N, Berjanskii M,
696 Singhal S, Arndt D, Liang Y, Badran H, Grant J, Serra-Cayuela A, Liu Y, Mandal
697 R, Neveu V, Pon A, Knox C, Wilson M, Manach C, Scalbert A. 2018. HMDB 4.0:
698 the human metabolome database for 2018. Nucleic Acids Res 46:D608–D617.
699 36. Smith AM, Harrison JS, Sprague KM, Roy H. 2013. A conserved hydrolase
700 responsible for the cleavage of aminoacylphosphatidylglycerol in the membrane
701 of *Enterococcus faecium*. J Biol Chem 288:22768–22776.
702 37. Roy H. 2009. Tuning the properties of the bacterial membrane with aminoacylated
703 phosphatidylglycerol. IUBMB Life 61:940–953.
704 38. Ernst CM, Staubitz P, Mishra NN, Yang S-J, Hornig G, Kalbacher H, Bayer AS,
705 Kraus D, Peschel A. 2009. The Bacterial Defensin Resistance Protein MprF
706 Consists of Separable Domains for Lipid Lysinylation and Antimicrobial Peptide
707 Repulsion. PLoS Pathog 5:e1000660.
708 39. Ernst CM, Slavetinsky CJ, Kuhn S, Hauser JN, Nega M, Mishra NN, Gekeler C,
709 Bayer AS, Peschel A. 2018. Gain-of-function mutations in the phospholipid
710 flippase mprf confer specific daptomycin resistance. MBio 9:1–12.
711 40. Spencer BL, Deng L, Patras KA, Burcham ZM, Sanches GF, Nagao PE, Doran
712 KS. 2019. Cas9 contributes to Group B Streptococcal colonization and disease.
713 Front Microbiol 10:1–15.
714 41. Deng L, Spencer BL, Holmes JA, Mu R, Rego S, Weston TA, Hu Y, Sanches GF,
715 Yoon S, Park N, Nagao PE, Jenkinson HF, Thornton JA, Seo KS, Nobbs AH,
716 Doran KS. 2019. The Group B Streptococcal surface antigen I/II protein, BspC,

717 interacts with host vimentin to promote adherence to brain endothelium and
718 inflammation during the pathogenesis of meningitis. PLoS Pathog 15:e1007848.
719 42. Banerjee A, Kim BJ, Carmona EM, Cutting AS, Gurney MA, Carlos C, Feuer R,
720 Prasadarao N V., Doran KS. 2011. Bacterial Pili exploit integrin machinery to
721 promote immune activation and efficient blood-brain barrier penetration. Nat
722 Commun 2:462.
723 43. Kim BJ, Hancock BM, Bermudez A, Del Cid N, Reyes E, van Sorge NM, Lauth X,
724 Smurthwaite CA, Hilton BJ, Stotland A, Banerjee A, Buchanan J, Wolkowicz R,
725 Traver D, Doran KS. 2015. Bacterial induction of Snail1 contributes to blood-brain
726 barrier disruption. J Clin Invest 125:2473–83.
727 44. Bhardwaj P, Hans A, Ruikar K, Guan Z, Palmer KL. 2018. Reduced Chlorhexidine
728 and Daptomycin Susceptibility in Vancomycin-Resistant *Enterococcus faecium*
729 after Serial Chlorhexidine Exposure. Antimicrob Agents Chemother 62.
730 45. Poyart C, Pellegrini E, Marceau M, Baptista M, Jaubert F, Lamy MC, Trieu-Cuot
731 P. 2003. Attenuated virulence of *Streptococcus agalactiae* deficient in D-alanyl-
732 lipoteichoic acid is due to an increased susceptibility to defensins and phagocytic
733 cells. Mol Microbiol 49:1615–1625.
734 46. Kinjo Y, Illarionov P, Vela JL, Pei B, Girardi E, Li X, Li Y, Imamura M, Kaneko Y,
735 Okawara A, Miyazaki Y, Gómez-Velasco A, Rogers P, Dahesh S, Uchiyama S,
736 Khurana A, Kawahara K, Yesilkaya H, Andrew PW, Wong C-H, Kawakami K,
737 Nizet V, Besra GS, Tsuji M, Zajonc DM, Kronenberg M. 2011. Invariant natural
738 killer T cells recognize glycolipids from pathogenic Gram-positive bacteria. Nat
739 Immunol 12:966–74.

740 47. Zajonc DM, Girardi E. 2015. Recognition of microbial glycolipids by Natural Killer
741 T cells. Front Immunol 6:1–11.
742 48. Flannagan RS, Cosío G, Grinstein S. 2009. Antimicrobial mechanisms of
743 phagocytes and bacterial evasion strategies. Nat Rev Microbiol 7:355–66.
744 49. Miller EA, Beasley DAE, Dunn RR, Archie EA. 2016. Lactobacilli dominance and
745 vaginal pH: Why is the human vaginal microbiome unique? Front Microbiol 7.
746 50. Neugent ML, Hulyalkar N V., Nguyen VH, Zimmern PE, De Nisco NJ. 2020.
747 Advances in Understanding the Human Urinary Microbiome and Its Potential Role
748 in Urinary Tract Infection. MBio 11.
749 51. Slavetinsky CJ, Hauser JN, Gekeler C, Slavetinsky J, Kraus A, Heilingbrunner D,
750 Wagner S, Tesar M, Krismer B, Kuhn S, Ernst CM, Peschel A. Decoding and
751 blocking the bacterial lipid flippase MprF yields a novel anti-virulence strategy
752 [preprint] https://doi.org/10.1101/2020.11.12.379776.
753 52. Van De Rijn I, Kessler RE. 1980. Growth characteristics of Group A Streptococci
754 in a new chemically defined medium. Infect Immun 27:444–448.
755 53. Chang JC, LaSarre B, Jimenez JC, Aggarwal C, Federle MJ. 2011. Two Group A
756 Streptococcal peptide pheromones act through opposing rgg regulators to control
757 biofilm development. PLoS Pathog 7:e1002190.
758 54. Gupta R, Shah P, Swiatlo E. 2009. Differential gene expression in *Streptococcus*
759 *pneumoniae* in response to various iron sources. Microb Pathog 47:101–109.
760 55. Holo H, Nes IF. 1989. High-frequency transformation, by electroporation, of
761 *Lactococcus lactis* subsp. *cremoris* grown with glycine in osmotically stabilized
762 media. Appl Environ Microbiol 55:3119–3123.

763 56. Framson PE, Nittayajarn A, Merry J, Youngman P, Rubens CE. 1997. New
764 genetic techniques for Group B Streptococci: High-efficiency transformation,
765 maintenance of temperature-sensitive pWV01 plasmids, and mutagenesis with
766 Tn917. Appl Environ Microbiol 63:3539–3547.
767 57. Li C, Tan BK, Zhao J, Guan Z. 2016. In vivo and in vitro synthesis of
768 phosphatidylglycerol by an *Escherichia coli* cardiolipin synthase. J Biol Chem
769 291:25144–25153.
770 58. Gogos A, Jimenez J, Chang J, Wilkening R, Federle M. 2018. A Quorum Sensing-
771 Regulated Protein Binds Cell Wall *Streptococcus pyogenes*. J Bacteriol 200:1–16.
772 59. Kristian SA, Datta V, Weidenmaier C, Kansal R, Fedtke I, Peschel A, Gallo RL,
773 Nizet V. 2005. D-alanylation of teichoic acids promotes Group A *Streptococcus*
774 antimicrobial peptide resistance, neutrophil survival, and epithelial cell invasion. J
775 Bacteriol 187:6719–25.
776 60. Garrett TA, Raetz CRH, Son JD, Richardson TD, Bartling C, Guan Z. 2011. Non-
777 enzymatically derived minor lipids found in *Escherichia coli* lipid extracts. Biochim
778 Biophys Acta 1811:827–37.
779
780

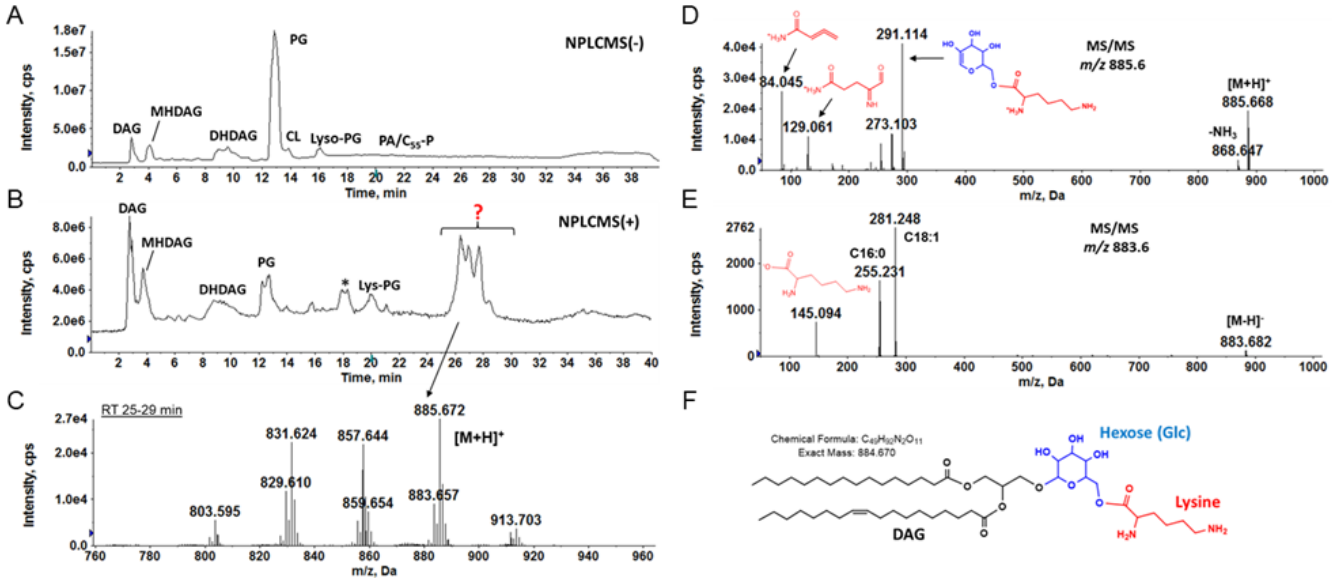

Figure 1. Lipidomic profiling identifies a major unknown lipid as Lysyl-Glucosyl-Diacylglycerol in GBS. The total lipid extract of the WT COH1 strain was analyzed by normal phase LC-ESI/MS in both negative and positive ion modes. A) Total ion chromatogram (TIC) of LC/MS in the negative ion mode shows common Gram-positive bacterial lipids. B) TIC of LC/MS in the positive ion mode shows a major unknown lipid eluting from the column at ~25 to 29 min. C) Positive ESI/MS showing the $[M+H]^+$ ions of the unknown lipid. The spectrum was averaged from those acquired during the retention time of 25 to 29 min. D) Positive ion MS/MS spectrum of $[M+H]^+$ at *m/z* 885.6 of the unknown lipid. E) Negative ion MS/MS spectrum of $[M-H]^-$ at *m/z* 883.6 of the unknown lipid. F) Lys-Glc-DAG (16:0/18:1) is proposed as the structure of the unknown lipid that gave rise to the $[M+H]^+$ at *m/z* 885.6 and $[M-H]^-$ at *m/z* 883.6. The hexose was assigned as glucose, because glucosyl-DAG is a major gram-positive membrane lipid and is supported by the isotopic labeling studies using a ^{13}C-labeled glucose shown below. The acyl chain compositions and exact masses of Lys-Glc-DAG molecular species observed in COH1 are listed in Table S1. "*" denotes methylcarbamate of Lys-Glc-DAG , an extraction artifact due to the use of chloroform (60).

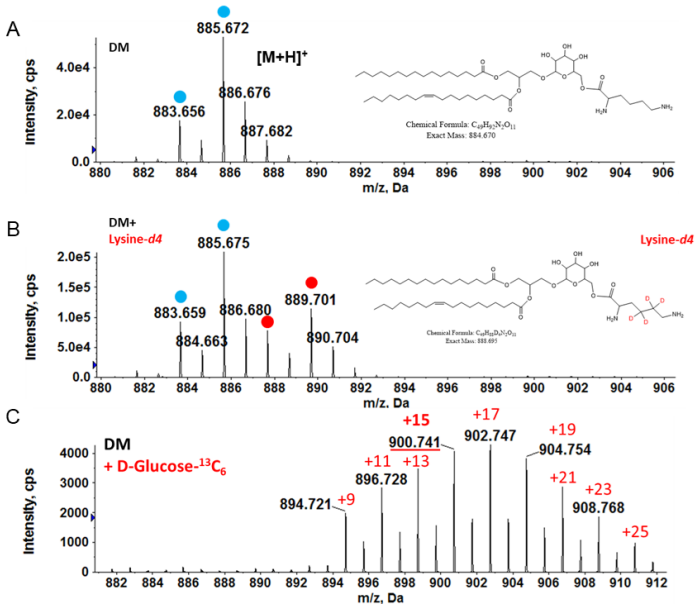

800 **Figure 2. Isotopic incorporation of deuterated lysine and ^{13}C-labeled glucose into**
801 **Lys-Glc-DAG.** The lipid extracts of COH1 cultured in DM, DM supplemented with 450 μM
802 L-lysine-*d4* (4,4,5,5-D4), or in DM containing 0.5% w/v D-Glucose (U-$^{13}C_6$) were analyzed
803 by LC-ESI/MS in the positive ion mode. A) $[M+H]^+$ ions of major Lys-Glc-DAG species in
804 COH1 cultured in DM. B) $[M+H]^+$ ions of major Lys-Glc-DAG species in COH1 cultured in
805 DM supplemented with lysine-*d4.* The incorporation of lysine-*d4* in Lys-Glc-DAG is
806 evidenced by an upward *m/z* shift of 4 Da from unlabeled Lys-Glc-DAG (blue dots) to
807 labeled Lys-Glc-DAG (red dots). C) $[M+H]^+$ ion of Lys-Glc-DAG (16:0/18:1) is observed
808 at multiple peaks with higher m/z values (from *m/z* 894.7 to 910.8) when *S. agalactiae*
809 COH1 is cultured in DM supplemented with D-Glucose-$^{13}C_6$. The mass shifts, ranging
810 from +9 to +25 Da, indicate the numbers of ^{13}C atoms that were incorporated into Lys-
811 Glc-DAG (16:0/18:1).

812

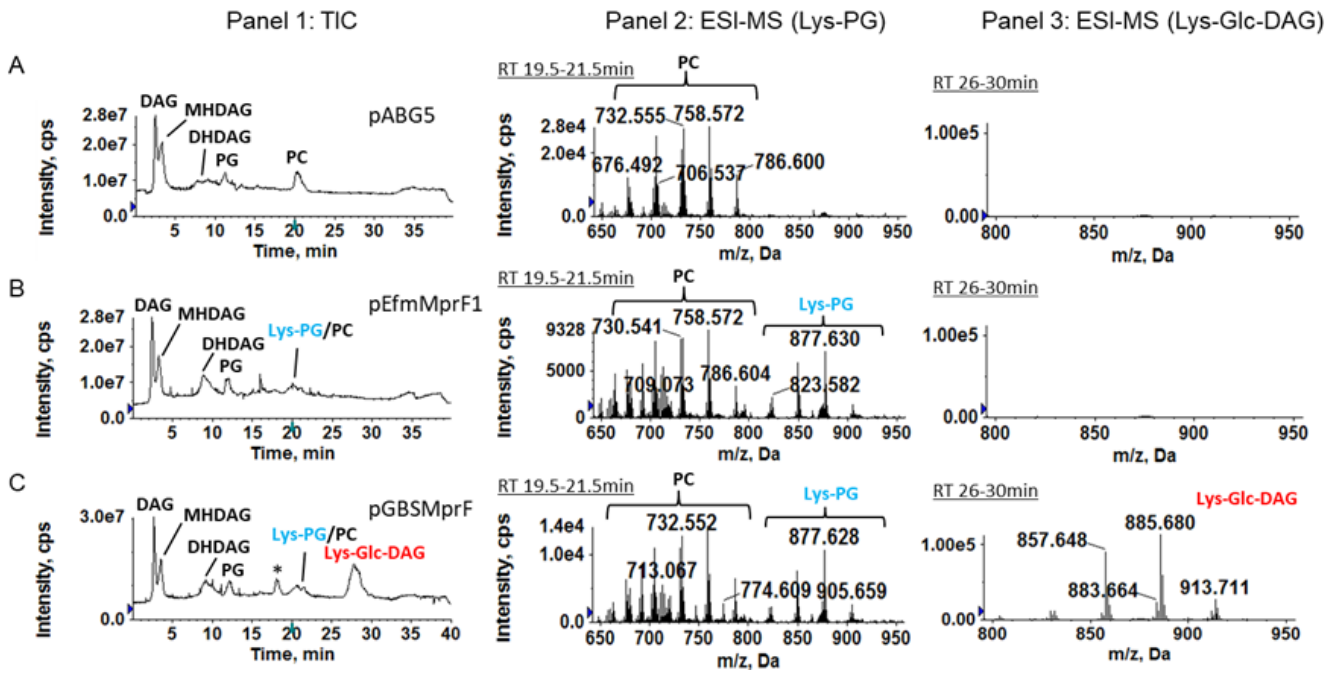

Figure 3. Expression of *E. faecium* MprF and GBS MprF in *S. mitis*. The lipid extracts of *S. mitis* ATCC 49456 cells with empty vector control (pABG5), expressing *E. faecium mprF1* (pEfmMprF1), and GBS *mprF* (pGBSMprF), were analyzed by LC-ESI/MS in the positive ion mode. Panel 1: Total ion chromatograms (TIC), Panel 2: Mass spectra (MS) of retention time 19.5 – 21.5 min showing Lys-PG, and Panel 3: MS of retention time 26 – 30 min for Lys-Glc-DAG. A) *S. mitis* (pABG5), B) *S. mitis* (pEfmMprF1), and C) *S. mitis* (pGBSMprF). Phosphatidylcholine (PC) elutes around the same retention time of Lys-PG. Lys-PG is present when *mprF* from either *E. faecium* or GBS are expressed. Lys-Glc-DAG is only synthesized by the GBS MprF, indicating two lipid substrates for the GBS MprF. "*" denotes methylcarbamate of Lys-Glc-DAG, an extraction artifact.

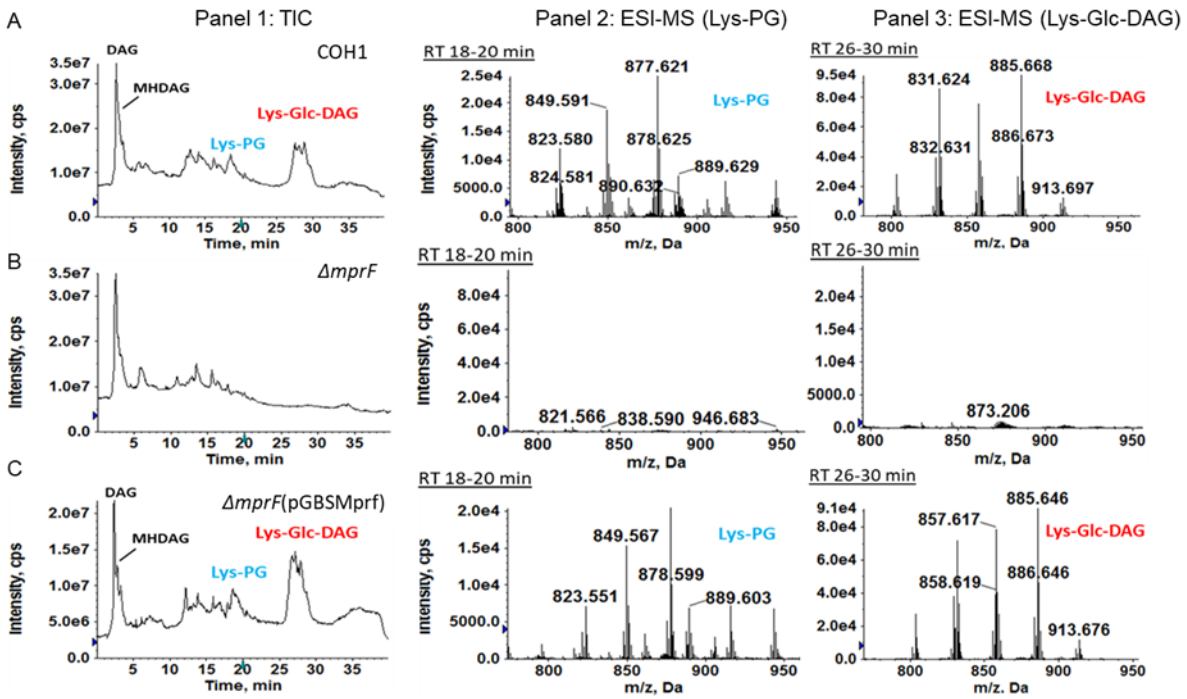

Figure 4. Deletion of *mprF* (GBSCOH1_1931) results in the loss of both Lys-PG and Lys-Glc-DAG from GBS. The lipid extracts of COH1 WT, COH1Δ*mprF* and Δ*mprF* (pGBSMprF) complement were analyzed by LC-ESI/MS in the positive ion mode. Panel 1: Total ion chromatograms (TIC), Panel 2: Mass spectra of retention time 18 – 20 min showing Lys-PG, and Panel 3: Mass spectra of retention time 26 – 30 min for Lys-Glc-DAG. A) COH1 WT, B) COH1Δ*mprF*, and C) Δ*mprF* (pGBSMprF) complement. The deletion of *mprF* from the COH1 genome results in a complete loss of both Lys-PG and Lys-Glc-DAG from the membrane, with both being restored in the complement strain, confirming MprF is the biosynthetic enzyme of both Lys-PG and Lys-Glc-DAG.

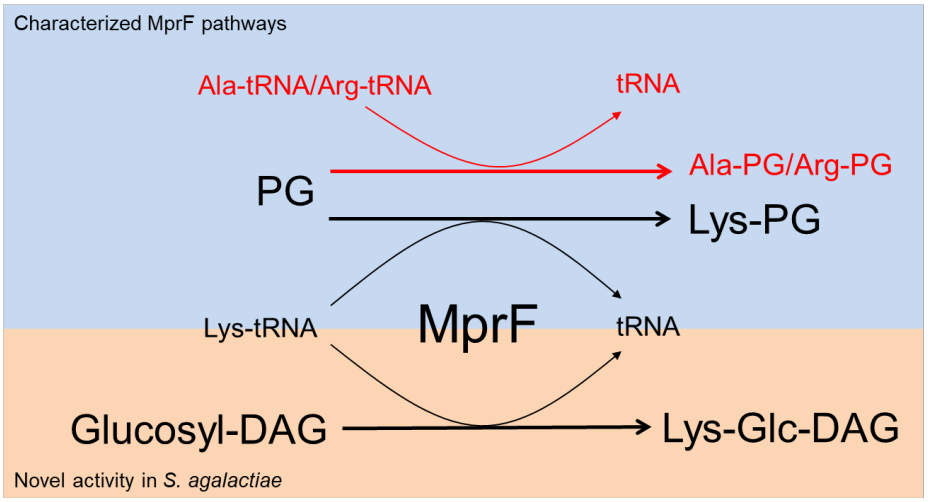

Figure 5. Biosynthetic pathways involving MprF. MprF has been demonstrated to catalyze the formation of Ala-PG, Arg-PG, and Lys-PG in many bacterial species (blue shading). In this study, we discover a novel function of MprF in GBS in the formation of Lys-Glc-DAG (orange shading). The biosynthetic pathways of MprF in GBS are denoted in black. Ala-PG and Arg-PG (formed by the pathway denoted in red) are not detected in GBS.

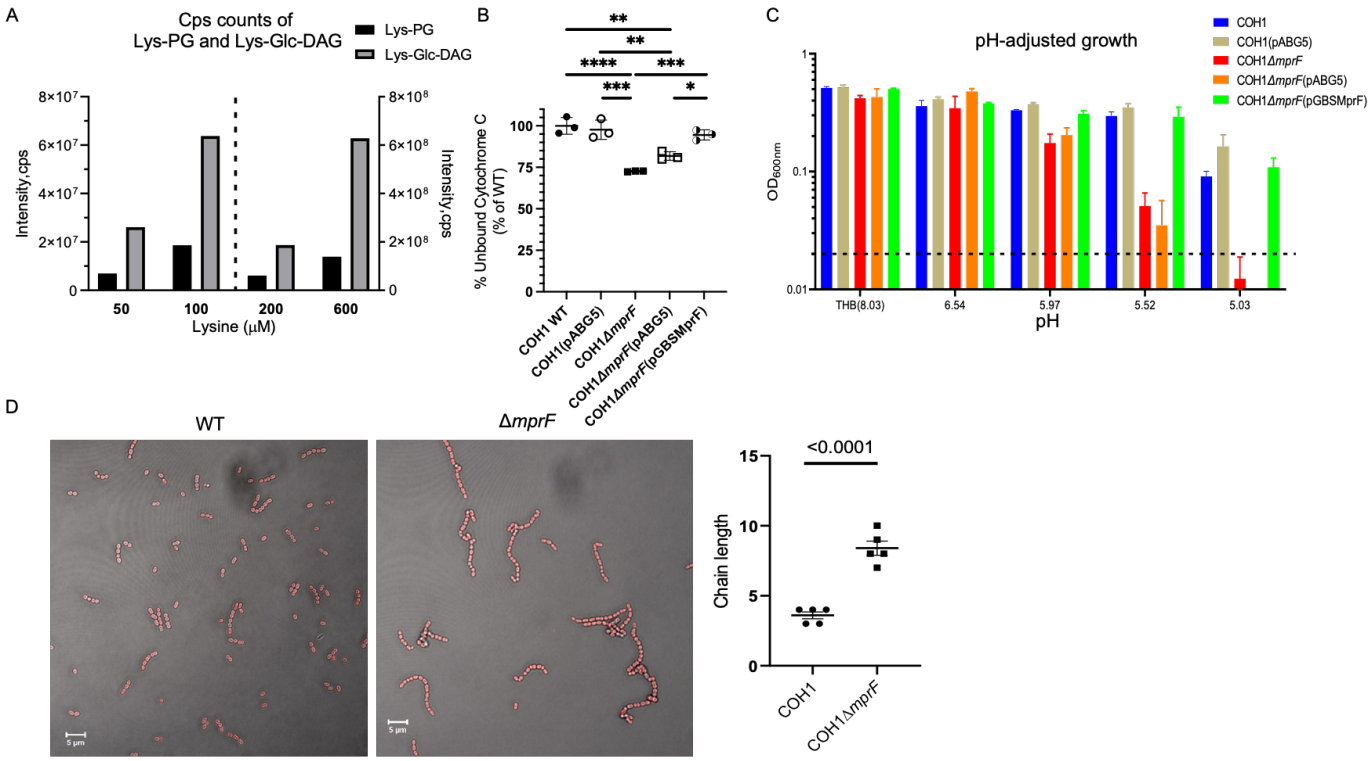

Figure 6. Lysine titration and COH1Δ*mprF* surface charge, acid tolerance, and chain length. A) Counts per second (CPS) counts from mass spectra for Lys-PG and Lys-Glc-DAG molecular species at each concentration. B) Mean percent of unbound Cytochrome C to COH1 WT, WT containing the empty vector pABG5, Δ*mprF* mutant, Δ*mprF* mutant containing the empty vector, and the pGBSMprF complement strains with COH1 WT set to 100%. The Δ*mprF* mutant displays significantly more Cytochrome C bound to the cells, indicating a more net negative outer surface charge. C) Growth yields (OD_{600nm}) after overnight culture in pH-adjusted THB broth. The Δ*mprF* mutant is more susceptible to the lower pH and fails to grow at pH 5 compared to the WT and complement. Dashed line represents starting inoculum of OD_{600nm} ~0.02. D) Representative image of stationary phase COH1 WT and Δ*mprF* mutant stained with membrane dye FM4-64 and manual counts of the number of diplococci in each chain imaged in the 5 images taken from each slide. Scale bar is 5 μm. B) and D) Mean and SEM, C) Mean and SD indicated. Statistical analysis: B) One-way ANOVA with Tukey's multiple comparisons test; *, p-value < 0.05; **, p-value < 0.01; ***, p-value < 0.001; ****, p-value < 0.0001; D) unpaired two-tailed t-test, p-value indicated.

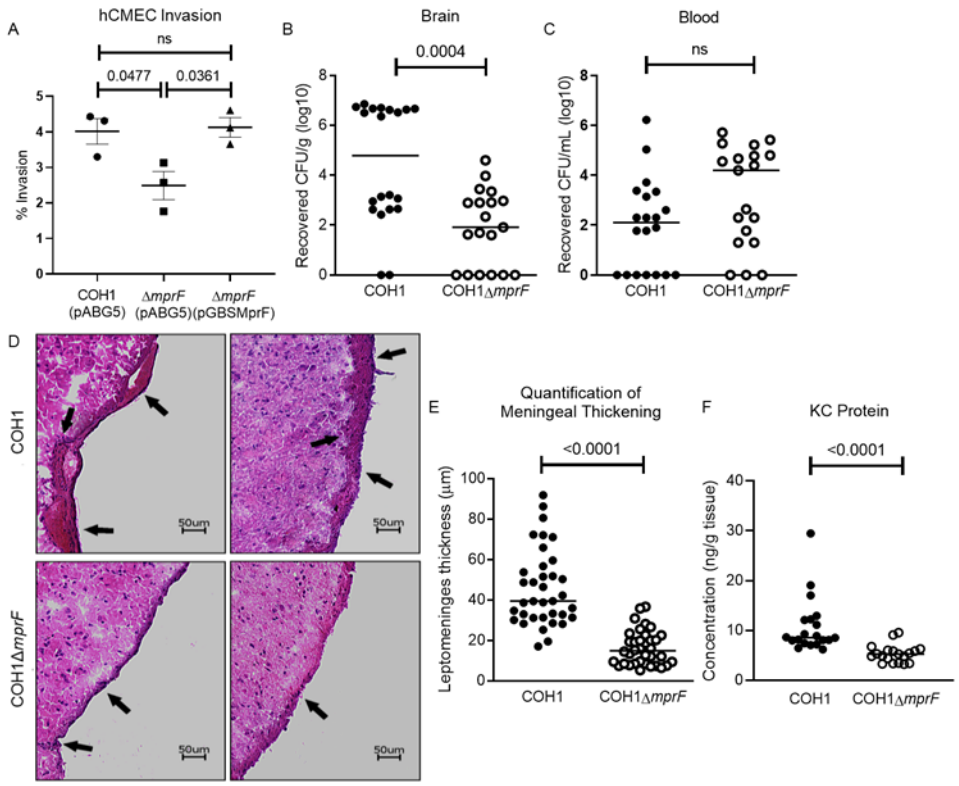

Figure 7. MprF contributes to human cell invasion and GBS meningitis *in vivo*. COH1(pABG5), Δ*mprF*(pABG5), and complement strain Δ*mprF*(pGBSMprF) were tested for A) invasion of the human cerebral endovascular hCMEC/DE3 cell line. The Δ*mprF*(pABG5) strain displays a significant difference in invasion of brain endothelium when compared to WT and complement strains. Groups of CD-1 mice (n = 9-10 per group) were injected intravenously with 1 x 10^9 CFU COH1 WT or COH1Δ*mprF* mutant strains. Representative data from 2 independent experiments are shown (*n* = 20 for WT and *n* = 19 for Δ*mprF* mutant). Mice were sacrificed after 72 h and bacterial counts were assessed in the B) brain and C) blood. D) Histopathology of hematoxylin-eosin-stained brain sections from representative mice infected with COH1 WT (top panels) or COH1Δ*mprF* mutant (bottom panels), arrows indicate areas of meningeal thickening and leukocyte infiltration. E) Quantification of meningeal thickening using ImageJ. E) KC chemokine production in brain tissue was measured by ELISA. *In vitro* tissue culture assay results are the mean of three replicate experiments, each with four technical replicates. Mean and SEM indicated. In panels B), C), E), and F) the bar indicates the Median. Statistical analyses: A) One-way ANOVA with Tukey's multiple comparisons test, B), C), and E) unpaired two-tailed t-test, F) Mann-Whitney U test, p-values indicated, and ns indicates no significance (p-value > 0.05).

883 **Table 1. Phospholipids and glycolipids present in strains used in this study[1].**

Species	Strain	Lipids						
		PA	PG	CL	Lys-PG	Lys-Glc-DAG	MHDAG	DHDAG
GBS	COH1	+	+	+	+	+	+	+
	A909	+	+	+	+	+	+	+
	CNCTC 10/84	+	+	+	+	+	+	+
	COH1Δ*mprF*	+	+	+	-	-	+	+
	COH1Δ*mprF*(pGBSMprF)	+	+	+	+	+	+	+
	COH1Δ*mprF*(pABG5Δ*phoZ*)	+	+	+	-	-	+	+
	COH1(pABG5Δ*phoZ*)	+	+	+	+	+	+	+
S. mitis	ATCC 49456(pABG5Δ*phoZ*)	+	+	+	-	-	+	+
	ATCC 49456(pGBSMprF)	+	+	+	+	+	+	+
	ATCC 49456(pEfmMprF1)	+	+	+	+	-	+	+
	ATCC 49456(pEfmMprF2)	+	+	+	-	-	+	+

884 [1]Abbreviations: GBS, Group B *Streptococcus*; PA, phosphatidic acid; PG,
885 phosphatidylglycerol; CL, cardiolipin; Lys-PG, lysyl-phosphatidylglycerol; Lys-Glc-DAG,
886 lysyl-glucosyl-diacylglycerol; MHDAG, monohexosyldiacylglycerol; DHDAG,
887 dihexosyldiacylglycerol.

888

889

Supplementary Text, Figures, and Tables

Streptococcus agalactiae MprF synthesizes a novel cationic glycolipid and plays a role in brain entry and meningitis

Luke R. Joyce[1], Haider S. Manzer[2], Jéssica da C. Mendonça[2], Ricardo Villarreal[2], Kelly S. Doran[2*], Kelli L. Palmer[1*], and Ziqiang Guan[3*]

[1]Department of Biological Sciences, The University of Texas at Dallas, Richardson, TX, 75080

[2]Department of Immunology and Microbiology, University of Colorado School of Medicine, Aurora, CO, 80045

[3]Department of Biochemistry, Duke University Medical Center, Durham, NC, 27710

*Corresponding authors

19 **Supplementary Text S1**

20 **Construction of MprF expression plasmids**

21 Genomic DNA was isolated using the Qiagen DNeasy Blood and Tissue kit per the
22 manufacturer's protocol with the exception that cells were pre-treated with 180 µL 50
23 mg/mL lysozyme, 25 µL 2500 U/mL mutanolysin, and 15 µL 20 mg/mL pre-boiled RNase
24 A and incubated at 37°C for 2 h. The *mprF* genes from GBS COH1, (GBSCOH1_1931),
25 and *E. faecium* 1,231,410 (EFTG_00601 and EFTG_02430) were amplified and Gibson
26 ligated into pABG5Δ*phoZ* (1). Plasmid constructs were transformed into chemical
27 competent *E. coli* DH5α cells. Briefly, chemically competent cells were incubated for 10
28 min on ice with 5 µL of Gibson reaction before heat shock at 42°C for 70 sec, then placed
29 on ice for 2 min before 900 µL of cold SOC medium was added. Outgrowth was performed
30 at 37°C, with shaking at 225 rpm, for 1 h. Cultures were plated on LB agar plates
31 containing 50 µg/mL kanamycin. Colonies were screened by PCR for presence of the
32 *mprF* insert.

33

34 **Construction of *mprF* deletion plasmid**

35 Regions ~2 kb upstream and downstream of the GBS COH1 *mprF* (GBSCOH1_1931)
36 were amplified using PCR (Supplementary Table 2). Plasmid, pMBSacB (2), and the PCR
37 products were digested using appropriate restriction enzymes and ligated overnight. 7 µL
38 of the ligation reaction was transformed into chemically competent *E. coli* DH5α as
39 described above, except that outgrowth was performed at 28°C with shaking at 225 rpm
40 for 90 min prior to plating on LB agar supplemented with 300 µg/mL erythromycin. Plates
41 were incubated at 28°C for 72 h. Colonies were screened by PCR for correct plasmid
42 construction. Positive colonies were inoculated into 50 mL LB media containing antibiotic

43 and incubated at 28°C with rotation at 225 rpm for 72 h. Cultures were pelleted using a
44 Sorvall RC6+ centrifuge at 4,280 x *g* for 6 min at room temperature. Plasmid was
45 extracted as described above except the cell pellet was split into 5 columns to prevent
46 overloading and serial eluted into 50 µL. Plasmid construction was confirmed via
47 restriction digest using XhoI and XbaI, and the insert was PCR amplified and sequence-
48 verified.
49
50 **Generation of electrocompetent GBS COH1 cells for *mprF* knockout**
51 Electrocompetent cells were generated as described (2) with minor modifications. Briefly,
52 a GBS COH1 colony was inoculated in 5 mL M17 medium (BD Bacto) with 0.5% glucose
53 and grown overnight at 37°C. The 5 mL was used to inoculate a second overnight culture
54 of 50 mL pre-warmed filter-sterilized M17 medium containing 0.5% glucose, 0.6% glycine,
55 and 25% PEG 8000. The second overnight was added to 130 mL of the same medium
56 and grown for 1 h at 37°C. Cells were pelleted at 3,200 x *g* in a Sorvall RC6+ at 4°C for
57 10 min. Cells were washed twice with 25 mL cold filter-sterilized GBS wash buffer
58 containing 25% PEG 8000 and 10% glycerol in water, and pelleted as above. Cell pellets
59 were re-suspended in 1 mL GBS wash buffer and either used immediately for
60 transformation or stored in 100 µL aliquots at -80°C until use.
61
62 **Complementation of *mprF* in COH1Δ*mprF***
63 Electrocompetent COH1Δ*mprF* were generated as previously described (3). Briefly,
64 COH1Δ*mprF* was inoculated into 5 mL THB with 0.6% glycine and grown overnight. The
65 culture was expanded to 50 mL in pre-warmed THB with 0.6% glycine and grown to an
66 OD_{600} nm of 0.3 and pelleted for 10 min at 3200 x *g* at 4°C in a Sorvall RC6+ floor

67 centrifuge. The pellet was kept on ice through the remainder of the protocol. The pellet
68 was washed twice with 25 mL and once with 10 mL of cold 0.625 M sucrose and pelleted
69 as above. The cell pellet was resuspended in 400 µL of cold 20% glycerol, aliquoted in
70 50 µL aliquots, and used immediately or stored at -80°C until use. Electroporation was
71 performed as described above, with recovery in THB supplemented with 0.25 M sucrose,
72 and plated on THB agar with kanamycin at 300 µg/mL.
73
74 **Acidic Bligh-Dyer extractions**
75 Centrifugation was performed using a Sorvall RC6+ centrifuge. Cultures were pelleted at
76 4,280 x *g* for 5 min at room temperature unless otherwise stated. The supernatants were
77 removed, and cell pellets were stored at -80°C until acidic Bligh-Dyer lipid extractions
78 were performed as described (4). Briefly, cell pellets were resuspended in 1X PBS
79 (Sigma-Aldrich) and transferred to Coring Pyrex glass tubes with PTFR-lined caps
80 (VWR), followed by 1:2 vol:vol chloroform:methanol addition. Single phase extractions
81 were vortexed periodically and incubated at room temperature for 15 minutes before 500
82 x *g* centrifugation for 10 min. A two-phase Bligh-Dyer was achieved by addition of 100 µL
83 37% HCl, 1 mL $CHCl_3$, and 900 µl of 1X PBS, which was then vortexed and centrifuged
84 for 5 min at 500 x *g.* The lower phase was removed to a new tube and dried under nitrogen
85 before being stored at -80°C prior to lipidomic analysis.
86
87 **Liquid Chromatography/Electrospray Ionization Mass Spectrometry**
88 Normal phase LC was performed on an Agilent 1200 quaternary LC system equipped
89 with an Ascentis silica HPLC column (5 µm; 25 cm by 2.1 mm; Sigma-Aldrich) as
90 described previously (5, 6). Briefly, mobile phase A consisted of chloroform-methanol-

91 aqueous ammonium hydroxide (800:195:5, vol/vol), mobile phase B consisted of
92 chloroform-methanol-water-aqueous ammonium hydroxide (600:340:50:5, vol/vol), and
93 mobile phase C consisted of chloroform-methanol-water-aqueous ammonium hydroxide
94 (450:450:95:5, vol/vol). The elution program consisted of the following: 100% mobile
95 phase A was held isocratically for 2 min, then linearly increased to 100% mobile phase B
96 over 14 min, and held at 100% mobile phase B for 11 min. The LC gradient was then
97 changed to 100% mobile phase C over 3 min, held at 100% mobile phase C for 3 min,
98 and, finally, returned to 100% mobile phase A over 0.5 min and held at 100% mobile
99 phase A for 5 min. The LC eluent (with a total flow rate of 300 µl/min) was introduced into
100 the ESI source of a high-resolution TripleTOF5600 mass spectrometer (Sciex,
101 Framingham, MA). Instrumental settings for negative-ion ESI and MS/MS analysis of lipid
102 species were: IS = -4,500 V, CUR = 20 psi, GSI = 20 psi, DP = -55 V, and FP = -150V.
103 Settings for positive-ion ESI and MS/MS analysis were: IS = +5,000 V, CUR = 20 psi, GSI
104 = 20 psi, DP = +55 V, and FP = +50V. The MS/MS analysis used nitrogen as the collision
105 gas. Data analysis was performed using Analyst TF1.5 software (Sciex, Framingham,
106 MA).
107
108 **Growth curves**
109 Overnight cultures were used to inoculate a 96 well flat-bottom plate (Falcon) at an
110 OD_{600nm} of ~0.02 in a final volume of 200 µL THB. Plates were grown in a Biotek MX
111 Synergy 2.0 plate reader at 37°C with OD_{600nm} readings every 15 minutes for 15 h. Growth
112 curves were performed in biological triplicate.
113
114 **Hemolytic assay**

115 Hemolytic assays were performed as described ((7)) with minor modifications. Briefly,
116 strains were grown to an OD_{600nm} of ~0.4, pelleted at 16,000 *x g* in an Eppendorf 5415D
117 tabletop centrifuge, and resuspended in PBS. ~8-9 x 10^7 CFU in 20 µL PBS was added
118 to 230 µL fresh sheep blood (VWR) in U-bottom 96-well plates (Corning) for a final volume
119 of 250 µL per well. Control wells were treated with 20 µL sterile water. The plates were
120 sealed and incubated at 37°C with rotation at 100 rpm for 1 h. The plates were centrifuged
121 at 400 x g for 10 min in an Eppendorf 5810 tabletop centrifuge, and 100 µL of the
122 supernatant was transferred to a flat-bottom 96-well plate (Falcon). 50 µL was diluted 1:2
123 in PBS and the absorbance at 541 nm (A_{541}) was read using a BioTek MX Synergy 2
124 plate reader. Percent hemolysis was calculated by comparing the A_{541} of GBS treated
125 wells to those of wells treated with water. Biological and technical replicates were
126 performed for each strain.
127
128

129

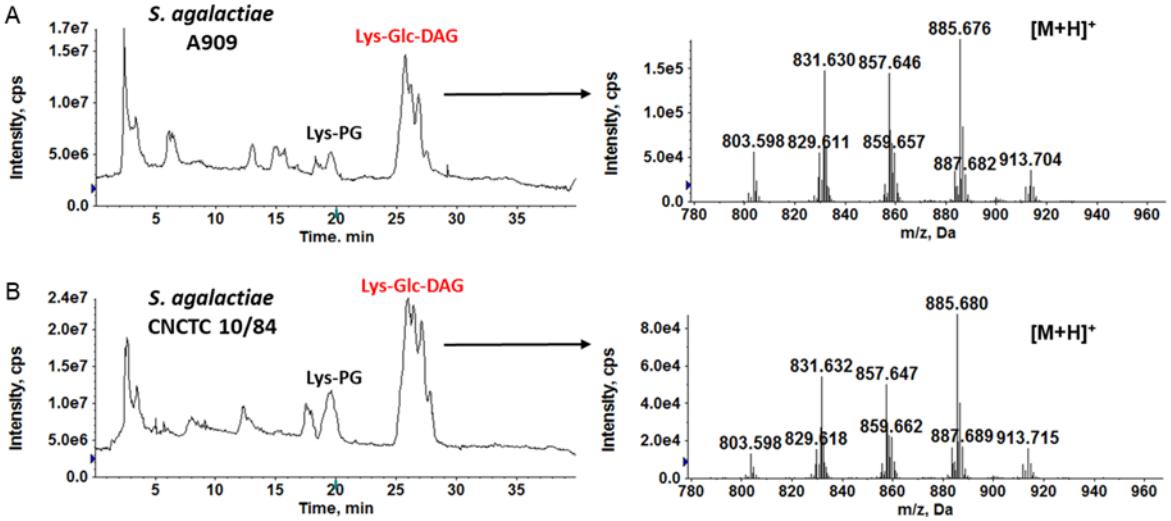

130 **Figure S1. Detection of Lys-PG and Lys-Glc-DAG in *S. agalactiae* A909 and *S.***
131 ***agalactiae* CNCTC 10/84.** Positive TICs (left panels) showing the presence of Lys-PG
132 and Lys-Glc-DAG in S*. agalactiae* A909 and S*. agalactiae* CNCTC 10/84. Mass spectra
133 (right panels) show the $[M+H]^+$ ions of Lys-Glc-DAG.

134

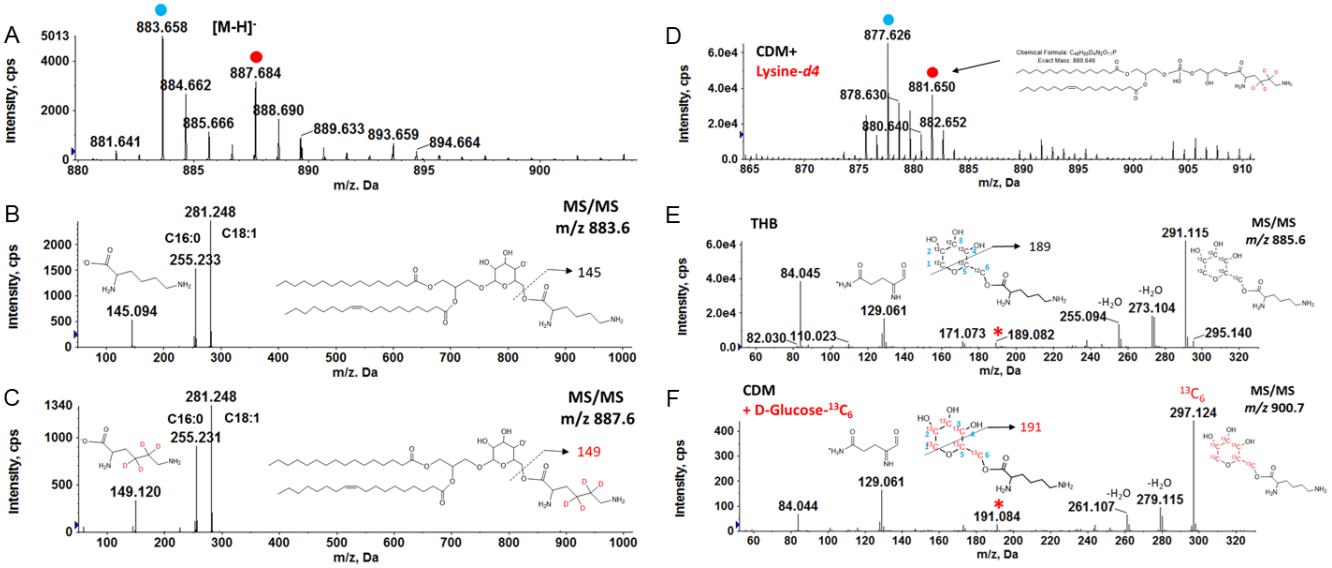

Figure S2. Isotopic incorporation of deuterated lysine and ^{13}C-labeled glucose into Lys-Glc-DAG and Lys-PG. The lipid extracts of *S. agalactiae* COH1 cultured in DM, DM supplemented with 450 μM L-lysine-*d4* (4,4,5,5-D4), or in DM containing 0.5% w/v D-Glucose (U-$^{13}C_6$) were analyzed by LC-ESI/MS in the positive ion mode. A) Negative ESI/MS of $[M-H]^-$ ions of major Lys-Glc-DAG species in *S. agalactiae* COH1 when cultured in DM supplemented with lysine-*d4*. The incorporation of lysine-*d4* into Lys-Glc-DAG is evidenced by an upward *m/z* shift of 4 Da of the $[M-H]^-$ ion (from *m/z* 883 to *m/z* 887). B) MS/MS of $[M-H]^-$ at *m/z* 883.6 produces a deprotonated lysine residue at *m/z* 145. C) MS/MS of $[M-H]^-$ at *m/z* 887.6 produces a deprotonated lysine-*d4* residue at *m/z* 149. D) $[M+H]^+$ ions of major Lys-PG species in *S. agalactiae* COH1 cultured in DM supplemented with lysine-*d4.* The incorporation of lysine-*d4* in Lys-PG is evidenced by an upward *m/z* shift of 4 Da from unlabeled Lys-PG (blue dot) to labeled Lys-PG (red dot). E) MS/MS of 885.6. A major product ion at *m/z* 291.1 is derived from glucose-lysine residue. F) MS/MS of *m/z* 900.7 (containing fifteen ^{13}C atoms). The presence of *m/z* 297.1 (with 6 Da shift) is consistent with glucose in Lys-Glc-DAG is replaced with D-Glucose (U-$^{13}C_6$). The other nine ^{13}C atoms are incorporated into the DAG portion of Lys-Glc-DAG. Furthermore, MS/MS data indicate that lysine is linked to the C6 position of glucose by the fragmentation schemes for forming *m/z* 189 ion from the unlabeled Lys-Glc-DAG and *m/z* 191 ion from the ^{13}C-labeled Lys-Glc-DAG.

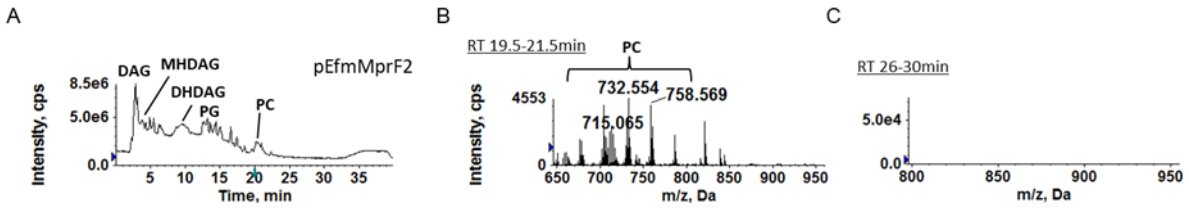

Figure S3. Neither Lys-PG nor Lys-Glc-DAG is produced by *E. faecium* MprF*2* expression in *S. mitis*. The lipid extracts of *S. mitis* (ATCC 49456) cells expressing *E. faecium mprF2* (pEfmMprF2) was analyzed by LC-ESI/MS in the positive ion mode. A) TIC of 49456(pEfmMprF2) shows the whole lipidomic profile. B) MS of retention time 19.5 – 21.5 min showing the absence of Lys-PG in the strain. C) MS of retention time 26 – 30 min showing the absence of Lys-Glc-DAG. This data is consistent with a previous report that the *mprF2* allele in the *E. faecium* genome is inactive (8).

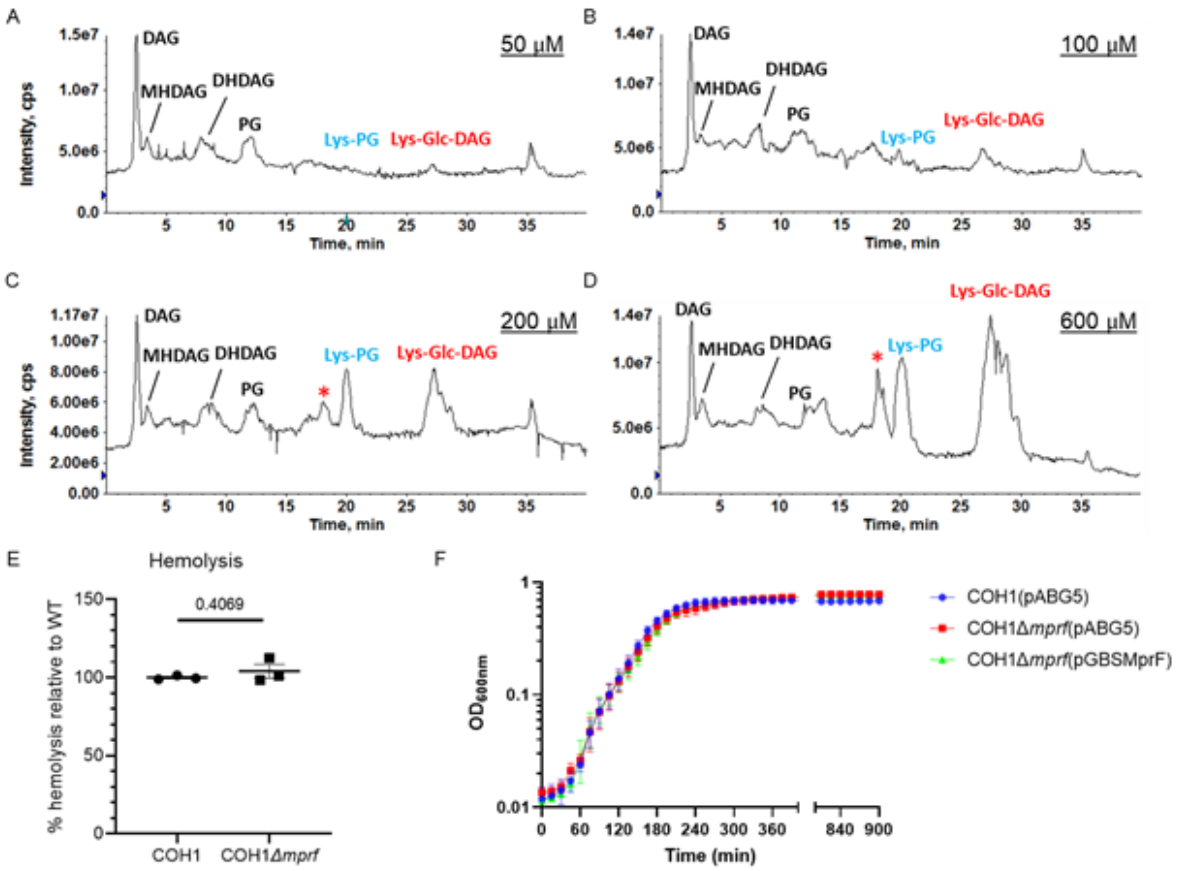

Figure S4. Lysine titration TICs and absence of hemolytic and growth phenotypes of COH1Δ*mprF* mutant. Shown are positive TICs of LC-ESI/MS of lipid extracts of COH1 cultured in defined growth media containing A) 50 µM lysine, B) 100 µM lysine, C) 200 µM lysine and D) 600 µM lysine. Lys-Glc-DAG and Lys-PG levels in COH1 positively correlate with lysine concentration in the growth medium. "*" denotes methylcarbamate, an extraction artifact of Lys-Glc-DAG. E) Hemolytic activity of WT COH1 and Δ*mprF* mutant. Mean and SEM indicated, statistical analysis: unpaired two-tailed t-test, p-value indicated. F) Growth curves of COH1(pABG5) (blue), COH1Δ*mprF*(pABG5) (red), and COH1Δ*mprF*(pGBSMprF) (green). There is no observable growth defect under these conditions. Mean and SD indicated.

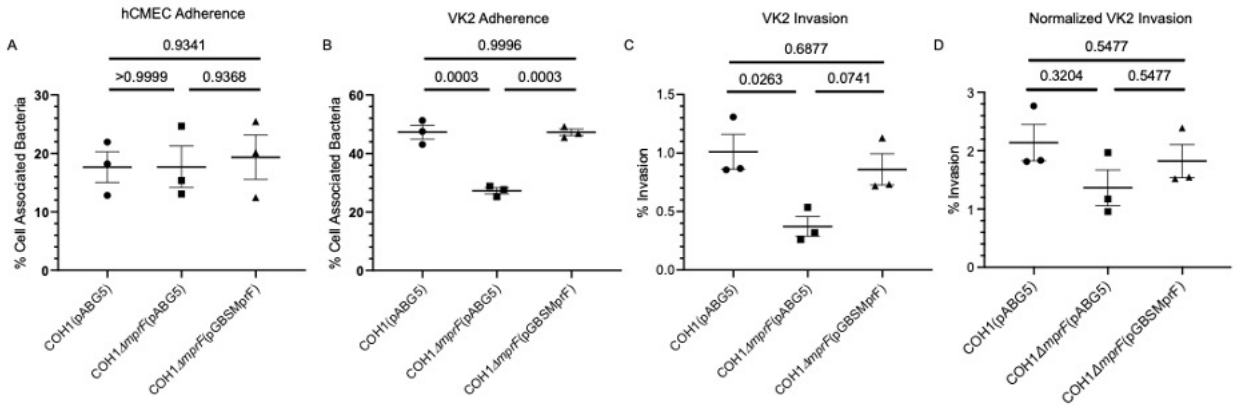

175

176 **Figure S5. MprF contributes to GBS adhesion and invasion of a cell lines *in vitro*.**
177 COH1(pABG5), Δ*mprF*(pABG5), and complement strain Δ*mprF*(pGBSMprF) were tested
178 for A) adhesion to human cerebral endovascular hCMEC/DE3 cell line and B) adhesion
179 and C) invasion of human vaginal epithelial VK2/E6E7 cell lines and D) percent invasion
180 of VK2/E6E7-associtated GBS. The Δ*mprF*(pABG5) strain displays no significant
181 difference in adhesion to hCMEC/DE3; however, the Δ*mprF*(pABG5) strain displays a
182 significant decrease in both adhesion and invasion compared to WT and complement
183 strains of the VK2/E6E7 cell line. The percent of VK2/E6E7-associated GBS that invaded
184 the cell suggests MprF contributes more to adhesion in this cell type. *In vitro* tissue culture
185 assay results are the mean of three replicate experiments, each with four technical
186 replicates. Mean and SEM indicated, statistical analyses: One-way ANOVA with Tukey's
187 multiple comparisons test, p-values indicated.

188 **Table S1. Observed and calculated exact masses of the $[M+H]^+$ ions of Lys-Glc-**
189 **DAG molecular species in *S. agalactiae* COH1.**

Lys-Glc-DAG[1]	$[M+H]^+$	
	Observed mass	Exact mass
C28:1	801.575	801.583
C28:0	803.595	803.599
C30:1	829.610	829.615
C30:0	831.624	831.630
C32:2	855.623	855.630
C32:1	857.644	857.646
C34:2	883.657	883.622
C34:1	885.672	885.677
C36:2	911.686	911.693
C36:1	913.703	913.709

199 [1]The numbers before and after colons indicate the total acyl chain carbon atoms and
200 double bonds, respectively.
201

202

203

204 **Table S2. Strains and plasmids used in this study.**

Organism	Strain	Description	Ref
S. agalactiae	ATCC BAA-1176 (COH1)	Wild-type *S. agalactiae* strain, serotype III	(9)
	COH1Δ*mprF*	*mprF* (GBSCOH1_1931) deletion strain	This work
	COH1Δ*mprF(*pABG5)	Empty vector control strain	This work
	COH1Δ*mprF*(pGBSMprf)	Expresses GBS *mprF* from P_{prtF} in pABG5Δ*phoZ*	This work
	COH1(pABG5)	Empty vector control	This work
	ATCC BAA-1138 (A909)	Wild-type *S. agalactiae* strain, serotype Ia	(10)
	CNCTC 10/84	Wild-type *S. agalactiae* strain, serotype V. Obtained from Dr. K Patras, UCSD	(11, 12)
S. mitis	ATCC 49456	Wild-type *S. mitis* type strain, also known as NCTC 12261	(13)
	ATCC 49456(pABG5)	Empty vector control	This work
	ATCC 49456(pGBSMprF)	Expresses GBS *mprF* from P_{prtF} in pABG5Δ*phoZ*	This work
	ATCC 49456(pEfmMprF1)	Expresses *E. faecium mprF1* from P_{prtF} in pABG5Δ*phoZ*	This work
	ATCC 49456(pEfmMprF2)	Expresses *E. faecium mprF1* from P_{prtF} in pABG5Δ*phoZ*	This work
E. coli	DH5α	Plasmid cloning host; F^-, φ80*lac*ZΔM15, *rec*A1, *end*A1, *hsd*R17, *pho*A, *sup*E44, λ^- *thi*-1, *gyr*A96, *rel*A1	(14)
	DH5α(pABG5)	Empty vector control	This work
	DH5α(pGBSMprF)	Expresses COH1 *mprF* (GBSCOH1_1931) from P_{prtF} in pABG5Δ*phoZ*	This work
	DH5α(pEfmMprF1)	Expresses *E. faecium mprF1* from P_{prtF} in pABG5Δ*phoZ*	This work
	DH5α(pEfmMprF2)	Expresses *E. faecium mprF1* from P_{prtF} in pABG5Δ*phoZ*	This work
	DH5α(pMBMprFKO)	Allelic exchange plasmid containing ~2 kb sequence flanking GBSCOH1_1931	This work
E. faecium	1,231,410	Wild type *E. faecium* strain	(15)

Plasmid	Description	Ref
pABG5Δ*phoZ*	Constitutive expression vector for streptococci with the P_{prtF} promoter. Confers kanamycin resistance. Referred to as pABG5 throughout the text	(1)
pGBSMprF	pABG5Δ*phoZ* expressing COH1 *mprF* (GBSCOH1_1931) from P_{prtF}	This work

pEfmMprF1	pABG5Δ*phoZ* expressing *E. faecium* 1,231,410 *mprF1* (EFTG_00601) from P_{prtF}	This work
pEfmMprF2	pABG5Δ*phoZ* expressing *E. faecium* 1,231,410 *mprF2* (EFTG_02430) from P_{prtF}	This work
pMBSacB	Allelic exchange plasmid for *S. agalactiae*. Confers erythromycin resistance and sucrose sensitivity	(2)
pMBMprFKO	Knockout plasmid containing ~2 kb sequence flanking GBSCOH1_1931	This work

205

206

207 **Table S3. Primers used in this study.**

Primer	5' – 3' sequence	Use
GBS_MprF_F	GAGAGGTCCCTTTCCTTGAAAAAGCTAATTGAAAAAGTC	Amplify GBSCOH1_1931 for Gibson assembly
GBS_MprF_R	ACCAATACCTTTATCTTATTTAACAATCTTAATTTTACTATC	Amplify GBSCOH1_1931 for Gibson assembly
Faec_MprF1_F	GAGAGGTCCCTTTCCTTGTTAAAAAATACCATACAATG	Amplify EFTG_00601 for Gibson assembly
Faec_MprF1_R	ACCAATACCTTTATCTTAATACTTTCTTCGTATCC	Amplify EFTG_00601 for Gibson assembly
Faec_MprF2_F	GAGAGGTCCCTTTCCGTGAAAAATAAACGATACTTG	Amplify EFTG_02430 for Gibson assembly
Faec_MprF2_R	ACCAATACCTTTATCTTATAATTCTGTGAGCACTTC	Amplify EFTG_02430 for Gibson assembly
pABG5-5'	GGAAAGGGACCTCTCTTCCTAAAC	Linearize pABG5Δ*phoZ* for Gibson assembly
pABG5-3'	GATAAAGGTATTGGTAAATAACAAA	Linearize pABG5Δ*phoZ* for Gibson assembly
	Expression plasmid sequencing	
GBS_S1	GAATGGAATAATATAGTAGGCT	For sequencing pGBSMprF, amplifies with pABG5_Fup2
GBS_S2	GATTGTATCCCTTATTCC	For sequencing pGBSMprF, amplifies with GBS_S3
GBS_S3	CGATTCAATAGCTTCAC	For sequencing pGBSMprF, amplifies with GBS_S2
GBS_S4	GATAAAAGGCTCTACTGG	For sequencing pGBSMprF, amplifies with pABG5_FDwn
pABG5_FDwn	CCAATAATAATGACTAGAGAAG	For pABG5 plasmid insert sequencing
pABG5_Fup2	CAAAAGGTTTCGACTTTTCACC	For pABG5 plasmid insert sequencing
EF1_S1	GAATAACGCTGATCAAAAGT	For sequencing pEfmMprF1, amplifies with pABG5_Fup2
EF1_S2	TGCCAAGAGAAATAGTC	For sequencing pEfmMprF1, amplifies with EF1_S3
EF1_S3	ACAATCTCTTCGCTTG	For sequencing pEfmMprF1, amplifies with EF1_S2
EF1_S4	CCAACTGTTCTTCTCCAA	For sequencing pEfmMprF1, amplifies with pABG5_FDwn
EF2_S1	CTCCTGTATGTGTGATGAAC	For sequencing pEfmMprF2, amplifies with pABG5_Fup2
EF2_S2	GGAATGGGGACTTTTGA	For sequencing pEfmMprF2, amplifies with EF2_S3
EF2_S3	ACTGATTCGTTGCTGC	For sequencing pEfmMprF2, amplifies with EF2_S2
EF2_S4	CTTCGCTTGTCAGGTTAC	For sequencing pEfmMprF2, amplifies with pABG5_FDwn
GBSCOH1_1931 knockout plasmid construction, sequencing, and integration screening		
Mp1F_PstI	ACGTCACTGCAGTTCAATTAGCTTTTTCAACAATTTC	Amplifies upstream fragment from within GBSCOH1_1931 leaving 6 codons, with Mp1R_XhoI
Mp1R_XhoI	ACGTCACTCGAGGCTGTTTATGGTGCTTTG	5' most primer of upstream fragment, amplifies with Mp1F_PstI
Mp2F_XbaI	ACGTCATCTAGAGAAAAGGCTAGATTACGAAC	3' most primer of downstream fragment, amplifies with Mp2R_PstI
Mp2R_PstI	ACGTCACTGCAGGTTAAATAAGCTTTATTTGGCA	Amplifies downstream fragment leaving 2 codons and stop codon of GBSCOH1_1931, with Mp2F_XbaI
T7 promoter	TAATACGACTCACTATAGGG	Amplifies with MpS5F below to sequence plasmid, amplifies with T3 promoter for insert screening and plasmid presence
T3 promoter	AATTAACCCTCACTAAAGGG	Amplifies with MpS3R below, amplifies with T7 promoter for insert screening and plasmid presence

Int_F	GCTAATTGAACTGCAGGTTAAATAAG	Anneals at *mprF* knockout site, amplifies with Out_R for single integration screening
Out_R	GCTATTATATTTAGTGGTTTAATTGG	Anneals outside recombination arms, amplifies with Int_F, for single integration screening
	Genomic knockout region sequencing	
MpS3F	CATTAGCTAGTCTTATCGGAG	Anneals outside integration arms, amplifies with MpS3R
MpS3R	ACAGCTACTTGGTAGTTCA	Amplifies with MpS3F
MpS4F	GCTACTAAGGCAAGATACG	Amplifies with MpS4R, knockout screening and plasmid sequencing primer
MpS4R	ATGGTCAGCGATGGTG	Amplifies with MpS4F, knockout screening and plasmid sequencing primer
MpS5F	CATAAGCGAAATAACTTGAG	Amplifies with MpS5R
MpS5R	GTATACAACGGCTTGATTGG	Anneals outside integration arms, amplifies with MpS5F

208

209

210 **References**

211 1. Granok AB, Parsonage D, Ross RP, Caparon MG. 2000. The RofA binding site in
212 *Streptococcus pyogenes* is utilized in multiple transcriptional pathways. J
213 Bacteriol 182:1529–40.

214 2. Hooven TA, Bonakdar M, Chamby AB, Ratner AJ. 2019. A Counterselectable
215 Sucrose Sensitivity Marker Permits Efficient and Flexible Mutagenesis in
216 *Streptococcus agalactiae*. Appl Environ Microbiol 85:1–13.

217 3. Framson PE, Nittayajarn A, Merry J, Youngman P, Rubens CE. 1997. New
218 genetic techniques for Group B Streptococci: High-efficiency transformation,
219 maintenance of temperature-sensitive pWV01 plasmids, and mutagenesis with
220 Tn917. Appl Environ Microbiol 63:3539–3547.

221 4. Joyce LR, Guan Z, Palmer KL. 2019. Phosphatidylcholine Biosynthesis in Mitis
222 Group Streptococci via Host Metabolite Scavenging. J Bacteriol 201:e00495-19.

223 5. Tan BK, Bogdanov M, Zhao J, Dowhan W, Raetz CRH, Guan Z. 2012. Discovery
224 of a cardiolipin synthase utilizing phosphatidylethanolamine and
225 phosphatidylglycerol as substrates. Proc Natl Acad Sci 109:16504–16509.

226 6. Li C, Tan BK, Zhao J, Guan Z. 2016. In vivo and in vitro synthesis of
227 phosphatidylglycerol by an *Escherichia coli* cardiolipin synthase. J Biol Chem
228 291:25144–25153.

229 7. Deng L, Spencer BL, Holmes JA, Mu R, Rego S, Weston TA, Hu Y, Sanches GF,
230 Yoon S, Park N, Nagao PE, Jenkinson HF, Thornton JA, Seo KS, Nobbs AH,
231 Doran KS. 2019. The Group B Streptococcal surface antigen I/II protein, BspC,
232 interacts with host vimentin to promote adherence to brain endothelium and
233 inflammation during the pathogenesis of meningitis. PLoS Pathog 15:e1007848.

234 8. Roy H, Ibba M. 2009. Broad range amino acid specificity of RNA-dependent lipid
235 remodeling by multiple peptide resistance factors. J Biol Chem 284:29677–29683.

236 9. Kuypers JM, Heggen LM, Rubens CE. 1989. Molecular analysis of a region of the
237 Group B *Streptococcus* chromosome involved in type III capsule expression.
238 Infect Immun 57:3058–65.

239 10. Lancefield RC, McCarty M, Everly WN. 1975. Multiple mouse-protective
240 antibodies directed against Group B Streptococci. Special reference to antibodies
241 effective against protein antigens. J Exp Med 142:165–79.

242 11. Wilkinson HW. 1977. Nontypable Group B Streptococci isolated from human
243 sources. J Clin Microbiol 6:183–4.

244 12. Hooven TA, Randis TM, Daugherty SC, Narechania A, Planet PJ, Tettelin H,
245 Ratner AJ. 2014. Complete Genome Sequence of *Streptococcus agalactiae*
246 CNCTC 10/84, a Hypervirulent Sequence Type 26 Strain. Genome Announc
247 2(6):e01338-14.

248 13. Kilian M, Mikkelsen L, Henrichsen J. 1989. Taxonomic Study of Viridans
249 Streptococci: Description of *Streptococcus gordonii* sp. nov. and Emended
250 Descriptions of *Streptococcus sanguis* (White and Niven 1946), *Streptococcus*
251 *oralis* (Bridge and Sneath 1982), and *Streptococcus mitis* (Andrewes and Horder
252 1906). Int J Syst Bacteriol 39:471–484.

253 14. Taylor RG, Walker DC, McInnes RR. 1993. *E. coli* host strains significantly affect
254 the quality of small scale plasmid DNA preparations used for sequencing. Nucleic
255 Acids Res 21:1677–1678.

256 15. Palmer KL, Carniol K, Manson JM, Heiman D, Shea T, Young S, Zeng Q, Gevers
257 D, Feldgarden M, Birren B, Gilmore MS. 2010. High-quality draft genome
258 sequences of 28 *Enterococcus* sp. isolates. J Bacteriol 192:2469–70.

259